Visual Abstract

Behavior of a Multi-Story Steel Structure with Eccentric X-Brace

Abdulkhalik J. Abdulridha
Department of Civil Engineering, College of Engineering, Al-Nahrain University, Jadriya, Baghdad, Iraq
Abdulkhalik.J.AbdulRidha@nahrainuniv.edu.iq, https://orcid.org/0000-0001-6403-2325

ABSTRACT. Eccentrically Braced Frames (EBFs) outperform moment-resisting frames in seismically active regions because of their strength, stiffness, energy dissipation, and ductility. Conventional bracing systems, such as X, Y, V, or K types, are utilized to enhance structural integrity. This study employs computational modelling to analyze multi-story steel buildings featuring an eccentric X-brace system. In this investigation, 120 multi-story steel frame buildings were selected. These multi-story structures comprise six-, nine-, and twelve-story geometries. ETABS built a full-scale FE model of multi-story structures. The study's parametric variables are the X-brace eccentricity, steel X-brace section size, and X-braced placement. Steel X-braces may have an eccentricity of 500, 1000, or 1500 millimeters. The ETABS model was validated when its findings matched experimental data. According to the data, the eccentric X-brace increases top-story displacement more for 6-story multi-story structures than for 9- and 12-story ones. Eccentric X-braces reduced lateral stiffness, allowing more significant floor movement. Eccentric and diagonal braces offer less lateral rigidity than concentrically braced frames due to their flexibility. Eccentricity reduces stiffness, even if the X-braced component has a larger cross-section. EBFs may migrate horizontally. Since the EBF absorbs more energy, changing the X-brace section size and eccentricity affects its ductility.

KEYWORDS. Eccentrically braced frames, EBFs, Numerical analysis, Seismic load, Eccentric X-braces, ETABS.

OPEN ACCESS

Citation: Abdulridha, A. J., Behavior of a Multi-Story Steel Structure with Eccentric X-Brace, Frattura ed Integrità Strutturale, 66 (2023) 273-296.

Received: 14.05.2023
Accepted: 29.08.2023
Online first: 01.09.2023
Published: 01.10.2023

INTRODUCTION

Steel Braced Frames (BFs) are commonly employed to provide rigidity and strength when subjected to lateral loading. During a seismic event, the steel-braced frames added to the structure dissipate energy. These frameworks deform plastically under tension and collapse under compression, whereas beams and columns are intended to remain in the elastic zone [1–4]. Eccentrically braced frames are a modern lateral force-resisting system designed to effectively and predictably sustain seismic events. As shown in Fig. 1, eccentric bracing employs braces that are not perpendicular to the columns or do not meet the floor beams. Buildings equipped with comprehensive and well-designed EBFs that are earthquake-resistant exhibit ductile behavior. The shear or flexural yielding of a connecting element provides evidence of this. The brace's eccentricity relative to the beam's midpoint or columns' centerlines may link them. Comprehensive and balanced hysteresis loops result from ductile yielding, which indicates exceptional energy dissipation. This quality is essential for resisting intense seismic activity. During seismic activity, horizontal forces are induced at the level of a structure's foundation, which can contribute to vibration issues. If the frequency of this excitation is comparable to the structure's inherent frequency, the vibrations can become quite powerful and result in resonance. So, this can result in significant displacement of the structure and even its collapse. [5–7]

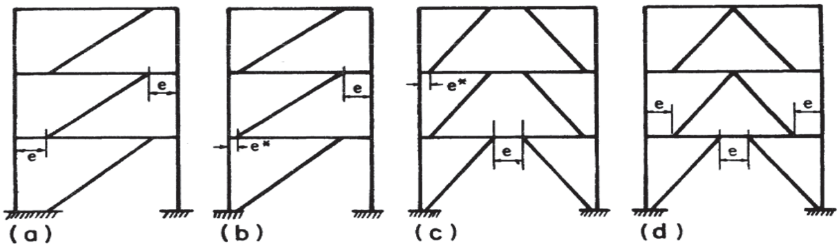

Figure 1: Alternative bracing configurations for EBFs [5].

Stratan et al. [8] conducted a cycle test on an eccentric brace using four different link lengths (e = 400, 500, 600, and 700 mm). Their findings show that the stiffeners' distance from one another in the joint significantly impacts their effectiveness. Short-range connections' speeds were controlled via web shear. As a result of the bolt coming loose at the shank, the lengthy links would have been more fragile. Popov and Engelhardt [5] concluded that the beam would fail if the link length to beam length ratio exceeded 0.5. Under the current conditions, the benefits of bracing are minimal. However, when the link length is shortened, the elasticity rises. Complexity increases in eccentric bracing connections compared to their simpler concentric counterparts, as seen in Fig. 2.

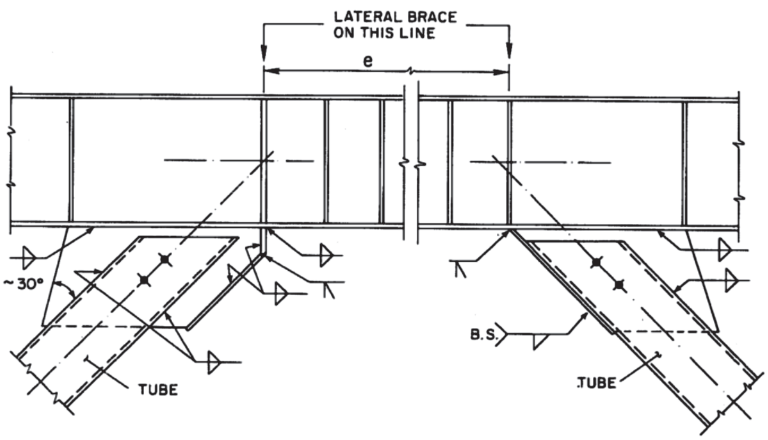

Figure 2: Typical eccentric construction bracing connections [5].

The initial stage of finite element modeling involves creating a geometric representation of the structure. Each element's material behavior and boundary conditions are divided into smaller forms. These smaller forms are connected to specific nodes, forming a mesh that is then analyzed [9–13]. It is essential to include computational modeling of the structure. The FE model can help with several tasks, such as finding the best place to put sensors, updating the model based on sensor measurements or a condensed model, measuring and locating structural changes (like damage), figuring out how reliable something is, and predicting how it will react under different simulated loading conditions. [14-21]
Concentric X-braced steel frames are popular due to their ability to withstand earthquakes and wind loads. The diagonals disperse seismic energy that would otherwise be lost by plasticizing under strain and bowing under compression. For instance, beams and columns are frequently designed to have flexibility [22, 24]. According to the American AISC 341-16 [23], we must consider the compressed diagonal. Failure to do so would result in a violation of the regulation. An elastic analysis has been requested [23, 25]. This study assumes that all bracing has the anticipated strength in tension or compression to withstand seismic activity before buckling. Considering the anticipated strength of the in-tension diagonal and the expected strength of the compressed diagonal post-buckling is necessary for the plastic analysis requested [23, 25]. The two phases of conduct are linked differently. Canadian [26] and Japanese [27] standards require two tests.

The previous studies primarily concentrated on eccentrically braced steel frames [28, 29]. Popov [30, 31] reviewed the current literature on EBFs and suggested various design modifications using the capacity design technique. Sullivan [32] proposed a design strategy based on direct displacement for eccentrically braced steel structures. This method considers the axial deformation of columns and supports and provides formulas for determining a structure's tale drift ratio and yield strength. Several studies [33–37] have examined the cyclic inelastic behavior of steel braces. These studies demonstrate that steel braces exhibit non-symmetrical hysteretic behavior, which includes strength loss under compressive stress and persistent deformations. Multiple experimental studies have demonstrated that steel reinforcements are prone to failure after repeated loading cycles. In addition, the effective buckling length and the elastoplastic properties of the material play a significant role in determining their reactivity [38–41]. Nip et al. [42] examined steel bracing with square and rectangular-shaped hollow cross-sections. The test results confirmed that the diagonal rods exhibit non-symmetrical hysteretic behavior and that their compressive strength decreases after a few compression cycles. Other investigations [43–45] have also found similar results.

MYTHOLOGY

Several EBF-related research has been undertaken, but they have yet to focus on the inquiry of eccentric X-braced steel frames, which is necessary here. El Centro seismic movements [46] are considered, along with 120 steel structural models. In this paper, eccentric X-braces in steel frames are the primary focus of the modeling efforts. The geometries of these high-rises range from 6 to 9 to 12 stories. The complex FE model of multi-story buildings was developed with the help of ETABS [47]. The parameters under study are the X-brace eccentricity, X-brace steel section size, and X-braced location. For steel X-braces, the eccentricity may range from 500 to 1500 mm. Each story's frame with eccentric X-braces is set at the building's corner (SC) and side (SS) to provide seismic force resistance in both orthogonal directions. Structure and architectural design information for multi-story structures are detailed on this page. It also discusses the static and dynamic properties of multi-story buildings in the context of a computer model.

SCHEMATIC OF EARTHQUAKE GROUND MOTIONS AND STRUCTURES

DESIGN OF ECCENTRIC X-BRACED FRAMES

This paper contains the study of G+6, G+9, and G+12 multi-story steel buildings beam column system with eccentric steel X-braces containing no shear walls subjected to the El-Centro earthquake [46] and modeled using ETABS V20, which is finite-element-based software [47] Modal frames built to ASCE 7 [48] standards for needed design strength and AISC 341 [23] standards for seismic design was analyzed in this work. All framing members are made of A992 steel with a yield strength of 345 MPa. In this study, the size of the building in the plan was 27.5 m x 27.5 m, each panel was a 5.5 m x 5.5 m square frame with a height of 3 m for each story and was constructed using H-shaped steel, and the X-braces were installed on the diagonals. In this study, there are a total of 120 buildings, with 40 being 6-story structures (18 m in height), 40 being 9-story structures (27 m in height), and the remaining 40 being 12-story structures (36 m in height).

The parametric study examines the eccentricity of steel X-braces, the size of the steel X-brace section, and the location of the X-brace. Three types of eccentricity of steel X-braces adopted are 500, 1000, and 1500 mm, respectively. The sections of the diagonal X-brace were H-shaped. Five steel section sizes (W-6x12, W-6x15, W-6x16, W-6x20, and W-6x25) were selected for the X-brace, and an adopted multi-story steel building with an X-brace section of W-6x16 was used as a control building to compare. The X-brace section's properties are shown in Tab. 1. There are two configurations of the location of the X-braces adopted in this study: EBFs in all stories are arranged at the corner on the perimeter of the buildings, and eccentric X-braces in all stories are arranged at the side on the perimeter of the buildings.

As seismic force-resisting systems in both orthogonal directions, the plan and 3D elevation of the studied 6-story, 9-story and 12-story with corner position of steel X-brace (SC) and side (SS) on the perimeter of the buildings, as depicted in Figs. 3 and 4, respectively. The alternative eccentricity of bracing arrangement of EBF's of steel buildings are shown in Fig. 5. Tabs. 2–3 illustrate the specifications of numbered steel structures with six-story, nine-story, and twelve-story heights and distinct X-brace sections. In order to transfer lateral stresses to the Concentric Braced Frames (CBFs) and EBFs, the floor system is made up of 100 mm thick concrete on a metal deck with steel shear bolts welded to floor beams and cast-in-place concrete decking with a "non-flexible" diaphragm. The x-type bracing system ensures the lateral stability of the building frame. The columns and girders of a "gravity-only frame" are joined utilizing shear beam-to-column connections (fully rigid), which can only support the weight of gravity. Dead and live loads for homes are expected to operate on the structure in addition to lateral stresses brought on by earthquake base excitation. Using the ETABS software, we determined the active gravity load to be (self-weight), and we set the superimposed dead load on each level to 2.5 kN/m2. The total live load, including the terrace, was calculated to be 4.79 kN/m2 using ASCE 7 [48].

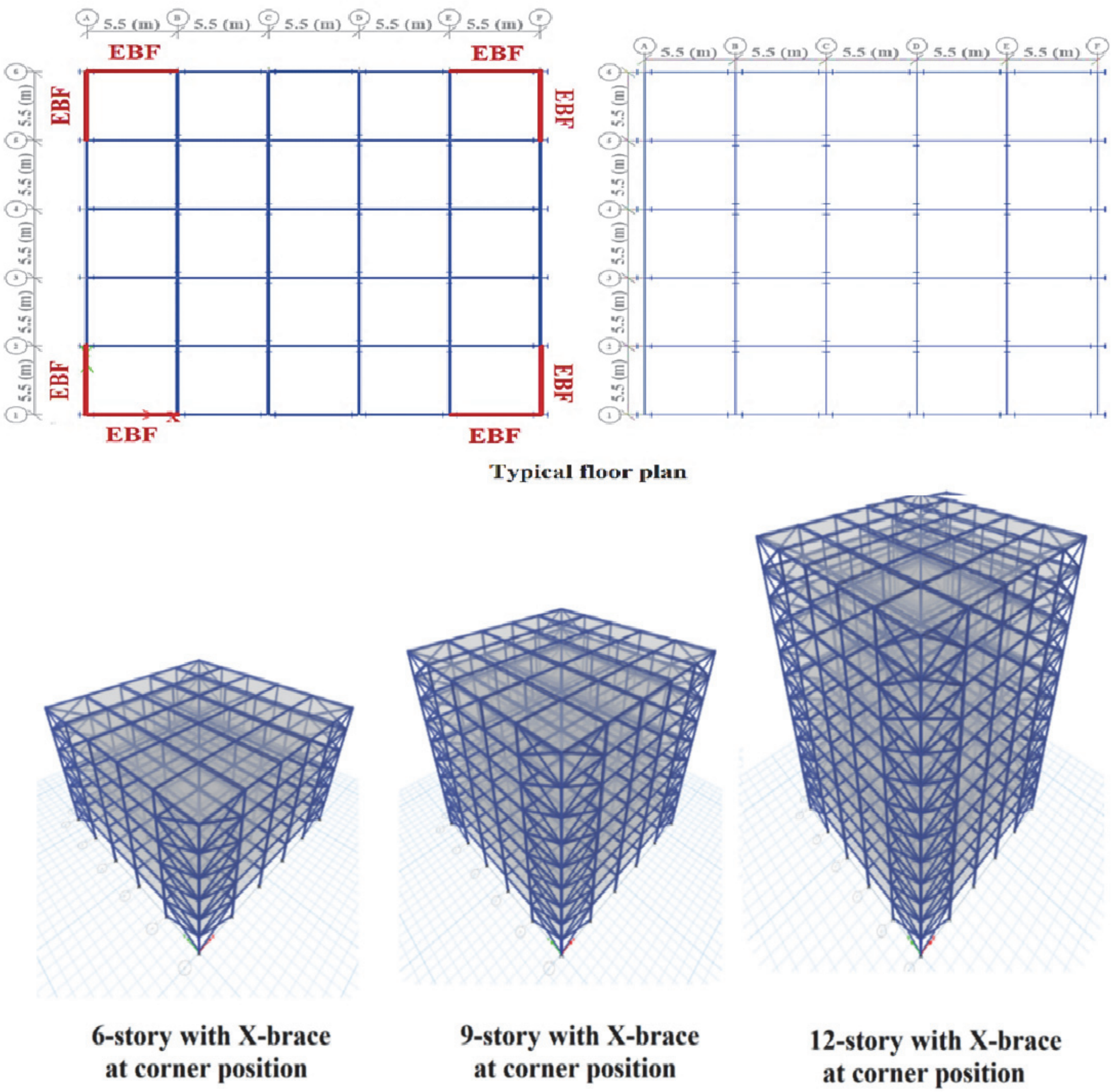

Figure 3: Plan and 3D elevation of the studied 6-story, 9-story and 12-story with corner position of steel X-brace (SC).

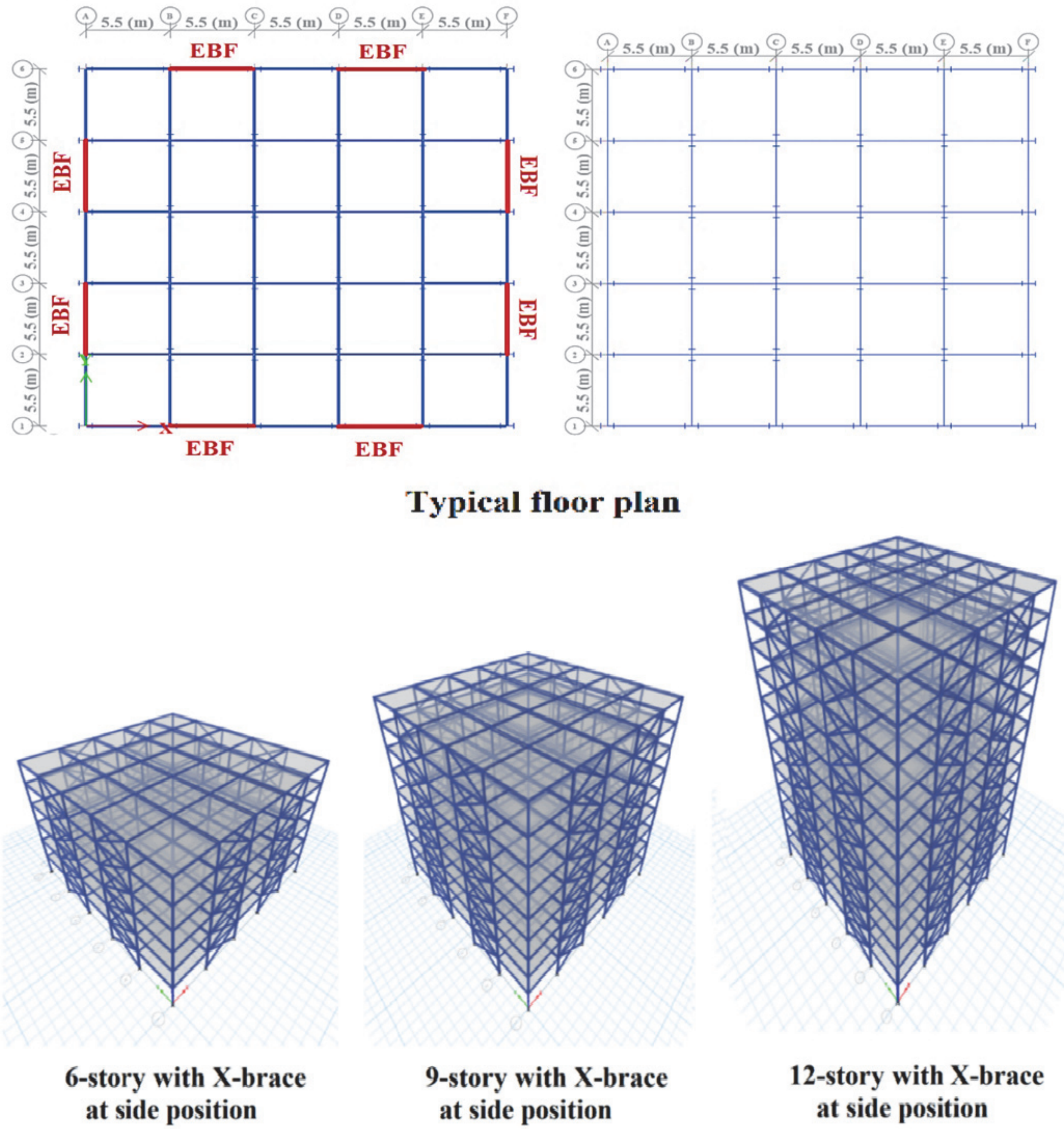

Figure 4: Plan and 3D elevation of the studied 6-story, 9-story and 12-story with side position of steel X-brace (SS).

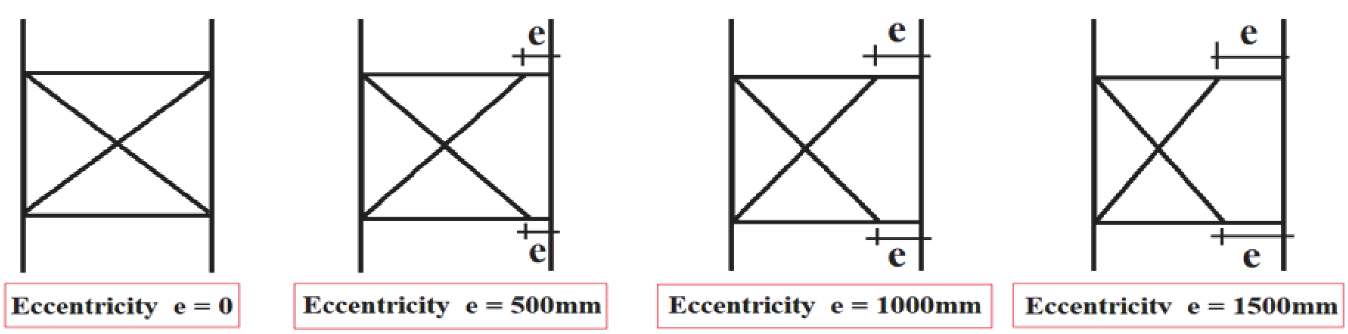

Figure 5: Alternative eccentricity of bracing arrangement of EBF's of steel buildings.

X-brace section	Area (mm2)	Depth (mm)	Web thickness (mm)	Flange width (mm)	Flange thickness (mm)	Ix (mm^4)	Iy (mm^4)	Sx (mm^3)	Sy (mm^3)	Zx (mm^3)	Zy (mm^3)	Weight (kg/m)	KL/r
W6x12	2290	153	5.84	102	7.11	9.2×10^6	1.24×10^6	120×10^3	24.6×10^3	136×10^3	38×10^3	18	6.24
W6x15	2860	152	5.84	152	6.6	12.1×10^6	3.88×10^6	159×10^3	51×10^3	177×10^3	77.8×10^3	22.5	3.47
W6x16	3060	160	6.6	102	10.3	13.4×10^6	1.84×10^6	167×10^3	36.1×10^3	192×10^3	55.6×10^3	24	6.59
W6x20	3790	157	6.6	153	9.27	17.2×10^6	5.54×10^6	220×10^3	72.3×10^3	246×10^3	110×10^3	29.8	3.63
W6x25	4740	162	8.13	154	11.6	22.2×10^6	7.12×10^6	274×10^3	91.9×10^3	310×10^3	140×10^3	37.1	3.97

Table 1: Details of the sections properties of steel X-brace (W-6x12, W-6x15, W-6x16, W-6x20 and W-6x25).

No. of story	Story No.	Eccentricity (mm)	X-brace position (Corner)				X-brace position (Side)			
			Building code	Beam section	Column section	Brace section	Building code	Beam section	Column section	Brace section
6	1	0	SC6-B16-1	W10x30	W8x24	W6x16	SS6-B16-1	W10x30	W8x24	W6x16
	2			W10x30	W8x24	W6x16		W10x30	W8x24	W6x16
	3			W10x30	W8x20	W6x16		W10x30	W8x20	W6x16
	4			W10x26	W8x20	W6x16		W10x26	W8x20	W6x16
	5			W10x26	W6x20	W6x16		W10x26	W6x20	W6x16
	6			W10x26	W6x20	W6x16		W10x26	W6x20	W6x16
9	1	0	SC9-B16-1	W10x33	W10x39	W6x16	SS9-B16-1	W10x33	W10x39	W6x16
	2			W10x33	W10x39	W6x16		W10x33	W10x39	W6x16
	3			W10x33	W10x39	W6x16		W10x33	W10x39	W6x16
	4			W10x30	W10x31	W6x16		W10x30	W10x31	W6x16
	5			W10x30	W10x31	W6x16		W10x30	W10x31	W6x16
	6			W10x30	W10x31	W6x16		W10x30	W10x31	W6x16
	7			W10x26	W8x31	W6x16		W10x26	W8x31	W6x16
	8			W10x26	W8x31	W6x16		W10x26	W8x31	W6x16
	9			W10x26	W8x31	W6x16		W10x26	W8x31	W6x16
12	1	0	SC12-B16-1	W10x39	W12x45	W6x16	SS12-B16-1	W10x39	W12x45	W6x16
	2			W10x39	W12x45	W6x16		W10x39	W12x45	W6x16
	3			W10x39	W12x45	W6x16		W10x39	W12x45	W6x16
	4			W10x33	W12x45	W6x16		W10x33	W12x45	W6x16
	5			W10x33	W10x39	W6x16		W10x33	W10x39	W6x16
	6			W10x33	W10x39	W6x16		W10x33	W10x39	W6x16
	7			W10x30	W10x39	W6x16		W10x30	W10x39	W6x16
	8			W10x30	W10x39	W6x16		W10x30	W10x39	W6x16
	9			W10x30	W8x35	W6x16		W10x30	W8x35	W6x16
	10			W10x26	W8x35	W6x16		W10x26	W8x35	W6x16
	11			W10x26	W8x35	W6x16		W10x26	W8x35	W6x16
	12			W10x26	W8x35	W6x16		W10x26	W8x35	W6x16

Table 2: Details of the members design of steel buildings with 6, 9 and 12-story with concentric X-brace.

No. of story	X-brace position	Eccentricity (mm)	e/L	Building code	Brace section	Building code	Brace section	Building code	Brace section	Building code	Brace section	Building code	Brace section
6	Corner	0	0	**SC6-B12-1**	W6x12	**SC6-B15-1**	W6x15	**SC6-B16-1**	W6x16	**SC6-B20-1**	W6x20	**SC6-B25-1**	W6x25
		500	0.094	**SC6-B12-2**	W6x12	**SC6-B15-2**	W6x15	**SC6-B16-2**	W6x16	**SC6-B20-2**	W6x20	**SC6-B25-2**	W6x25
		1000	0.188	**SC6-B12-3**	W6x12	**SC6-B15-3**	W6x15	**SC6-B16-3**	W6x16	**SC6-B20-3**	W6x20	**SC6-B25-3**	W6x25
		1500	0.282	**SC6-B12-4**	W6x12	**SC6-B15-4**	W6x15	**SC6-B16-4**	W6x16	**SC6-B20-4**	W6x20	**SC6-B25-4**	W6x25
	Side	0	0	**SS6-B12-1**	W6x12	**SS6-B15-1**	W6x15	**SS6-B16-1**	W6x16	**SS6-B20-1**	W6x20	**SS6-B25-1**	W6x25
		500	0.094	**SS6-B12-2**	W6x12	**SS6-B15-2**	W6x15	**SS6-B16-2**	W6x16	**SS6-B20-2**	W6x20	**SS6-B25-2**	W6x25
		1000	0.188	**SS6-B12-3**	W6x12	**SS6-B15-3**	W6x15	**SS6-B16-3**	W6x16	**SS6-B20-3**	W6x20	**SS6-B25-3**	W6x25
		1500	0.282	**SS6-B12-4**	W6x12	**SS6-B15-4**	W6x15	**SS6-B16-4**	W6x16	**SS6-B20-4**	W6x20	**SS6-B25-4**	W6x25
9	Corner	0	0	**SC9-B12-1**	W6x12	**SC9-B15-1**	W6x15	**SC9-B16-1**	W6x16	**SC9-B20-1**	W6x20	**SC9-B25-1**	W6x25
		500	0.094	**SC9-B12-2**	W6x12	**SC9-B15-2**	W6x15	**SC9-B16-2**	W6x16	**SC9-B20-2**	W6x20	**SC9-B25-2**	W6x25
		1000	0.188	**SC9-B12-3**	W6x12	**SC9-B15-3**	W6x15	**SC9-B16-3**	W6x16	**SC9-B20-3**	W6x20	**SC9-B25-3**	W6x25
		1500	0.282	**SC9-B12-4**	W6x12	**SC9-B15-4**	W6x15	**SC9-B16-4**	W6x16	**SC9-B20-4**	W6x20	**SC9-B25-4**	W6x25
	Side	0	0	**SS9-B12-1**	W6x12	**SS9-B15-1**	W6x15	**SS9-B16-1**	W6x16	**SS9-B20-1**	W6x20	**SS9-B25-1**	W6x25
		500	0.094	**SS9-B12-2**	W6x12	**SS9-B15-2**	W6x15	**SS9-B16-2**	W6x16	**SS9-B20-2**	W6x20	**SS9-B25-2**	W6x25
		1000	0.188	**SS9-B12-3**	W6x12	**SS9-B15-3**	W6x15	**SS9-B16-3**	W6x16	**SS9-B20-3**	W6x20	**SS9-B25-3**	W6x25
		1500	0.282	**SS9-B12-4**	W6x12	**SS9-B15-4**	W6x15	**SS9-B16-4**	W6x16	**SS9-B20-4**	W6x20	**SS9-B25-4**	W6x25
12	Corner	0	0	**SC12-B12-1**	W6x12	**SC12-B15-1**	W6x15	**SC9-B16-1**	W6x16	**SC9-B20-1**	W6x20	**SC9-B25-1**	W6x25
		500	0.094	**SC12-B12-2**	W6x12	**SC12-B15-2**	W6x15	**SC9-B16-2**	W6x16	**SC9-B20-2**	W6x20	**SC9-B25-2**	W6x25
		1000	0.188	**SC12-B12-3**	W6x12	**SC12-B15-3**	W6x15	**SC9-B16-3**	W6x16	**SC9-B20-3**	W6x20	**SC9-B25-3**	W6x25
		1500	0.282	**SC12-B12-4**	W6x12	**SC12-B15-4**	W6x15	**SC9-B16-4**	W6x16	**SC9-B20-4**	W6x20	**SC9-B25-4**	W6x25
	Side	0	0	**SS12-B12-1**	W6x12	**SS12-B15-1**	W6x15	**SS9-B16-1**	W6x16	**SS9-B20-1**	W6x20	**SS9-B25-1**	W6x25
		500	0.094	**SS12-B12-2**	W6x12	**SS9-B15-2**	W6x15	**SS9-B16-2**	W6x16	**SS9-B20-2**	W6x20	**SS9-B25-2**	W6x25
		1000	0.188	**SS12-B12-3**	W6x12	**SS9-B15-3**	W6x15	**SS9-B16-3**	W6x16	**SS9-B20-3**	W6x20	**SS9-B25-3**	W6x25
		1500	0.282	**SS12-B12-4**	W6x12	**SS9-B15-4**	W6x15	**SS9-B16-4**	W6x16	**SS9-B20-4**	W6x20	**SS9-B25-4**	W6x25

Table 3: Details of numerical steel buildings with 6, 9 and 12-story with various X-brace section.

THE FINITE ELEMENT MODEL USING ETABS

The finite element analysis program ETABS [47] is used extensively throughout this study to examine the structural behavior of the simulated steel building prototypes. The finite element model includes representations of the composite deck slab, central girders, steel bracings, secondary beams, and steel columns. The suggested structural models are three-dimensional finite element models. The composite slab is cut into shell elements for each panel in the "xy" plane, and the framing beams are cut into the same number of slab elements. The concrete on a metal deck slab with four-node shell components represents six degrees of freedom. Frame components are used to replicate the core girders, braces, secondary beams, and steel columns. The benefits of beam and truss components are combined in the frame element. In contrast to the beam element, which may deform in both shear and rotation at each edge, the truss element can only deform in one direction (axially). The time-history analysis is a method for investigating how a structure responds dynamically to varying loading over time. Time history dynamic analysis was performed to reproduce seismic base excitation by analyzing building models for ground acceleration time history of the EL-Centro earthquake ground motion [46]. In order to account for material nonlinearity and P-Δ effects in the study, a damping ratio of 5% was chosen. The inelastic behavior of the structural portion or system caused material nonlinearity. When a structural system is warped, P-Δ effects examine how well it can sustain a load in equilibrium.

GROUND ACCELERATION-TIME HISTORY DATA

The historic El-Centro (Imperial Valley) earthquake, estimated to have measured a magnitude of 7.1 on the Richter scale [46], posed an essential risk to these structures because of its relatively low peak ground acceleration (PGA) of 0.3 g. The letter g represents the acceleration due to gravity, which is 9.81 meters per second squared. The El-Centro earthquake was one of the earliest to collect extensive data on large-scale motion, making it a benchmark. Seismically safe construction codes, such as ASCE 7, were formed due to these studies. El-Centro's extensive motion data gave engineers crucial insights that helped them create buildings more resistant to earthquakes. For the following ASCE 7 [48] load combinations (the first equation was used for this study), Eqns. (1) through (4) may be used to depict the time dependence of the ground acceleration due to an earthquake:

$$1.2D + Ev + Eh + L + 0.15S \tag{1}$$

$$1.0D + 0.7Ev + 0.7Eh \tag{2}$$

$$1.0D + 0.525Ev + 0.525Eh + 0.75L + 0.1S \tag{3}$$

$$0.6D - 0.7Ev + 0.7Eh \tag{4}$$

Where D represents the dead load, L represents the live load, S represents the superimposed load, Ev represents the vertical seismic load effect, and Eh represents the horizontal seismic load effect.

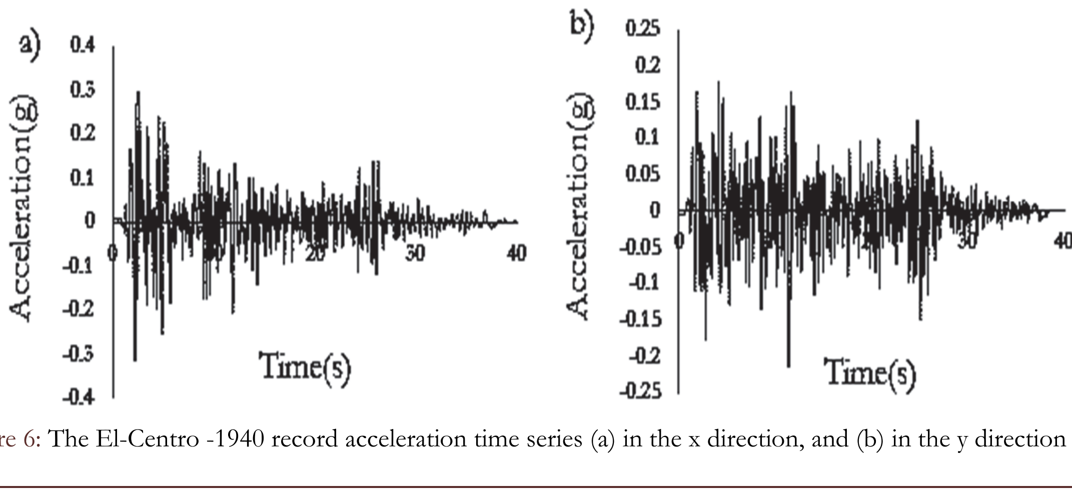

Figure 6: The El-Centro -1940 record acceleration time series (a) in the x direction, and (b) in the y direction [46].

Outline of experimental program

This work used the experimental study published by Alptug and Mevlut [49] to calibrate numerical findings and confirm their applicability; a short overview is given below. In Fig. 7, Alptug and Mevlut [49] show the features of a steel frame specimen indicative of their experimental test. Concentration was measured in single-bay, two-story, steel-braced buildings. The static lateral loading (pushover analysis) method was applied to an X-braced steel frame and specimens with a 100x100x3 mm cross-section. High-strength shafts were placed into the holes in the solid laboratory slab and then hammered into the ground to anchor the specimen firmly. Tab. 4 displays the profiles in a cross-section.

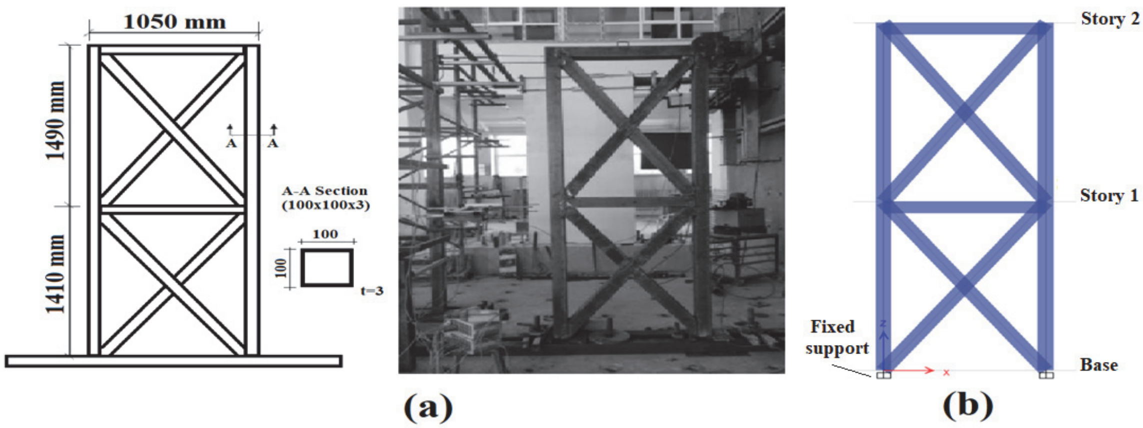

Figure 7: Details of steel frame specimen (a) experimental [49] and (b) ETABS.

Square section (mm)	Ax (mm^2)	Ix (mm^4)	Iy (mm^4)	ix (mm)	iy (mm)	W_{elx} (mm^3)	W_{ely} (mm^3)	W_{plx} (mm^3)	W_{ply} (mm^3)
100×100×3	1140	1.77*106	1.77*106	39.4	39.4	35400	35400	41200	41200

Table 4: Profile properties [49]

Conclusions and results - Certification results

A comparison of numerical and experimental data [49] is shown in Fig. 8. This graph shows how well the ETABS model fits with the experimental data. The ETABS to experimental axial compressive strength ratio (P_{Num}. / P_{Exp}) and the maximum longitudinal displacement (Δ_{Num} / Δ_{Exp}) fall between 1.03 and 1.04. Specimens exposed to stress testing are shown with experimental and numerical damage in Fig.9. The numerical technique correctly predicts the test frame's load-bearing capabilities, maximum displacement, and failure mechanism. Given that the samples differ by less than 10%. This finding is consistent with Harba and Abdulridha [50] and Risan et al. [51].

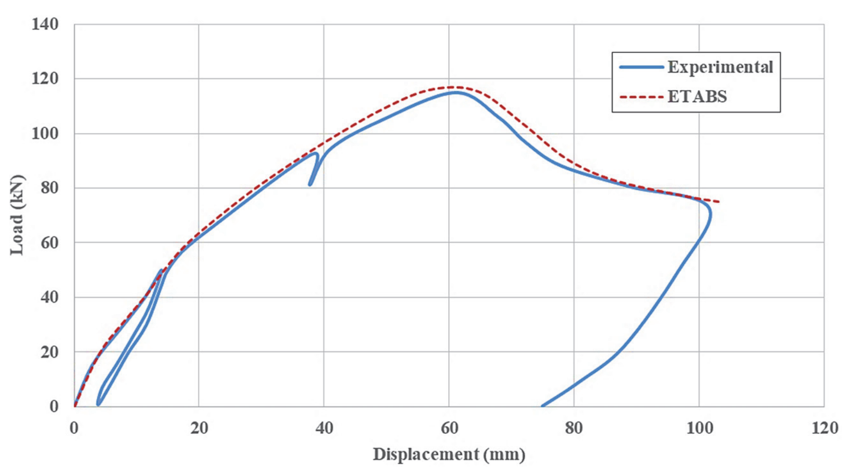

Figure 8: The experimental [49] and ETABS lateral load –displacement curves.

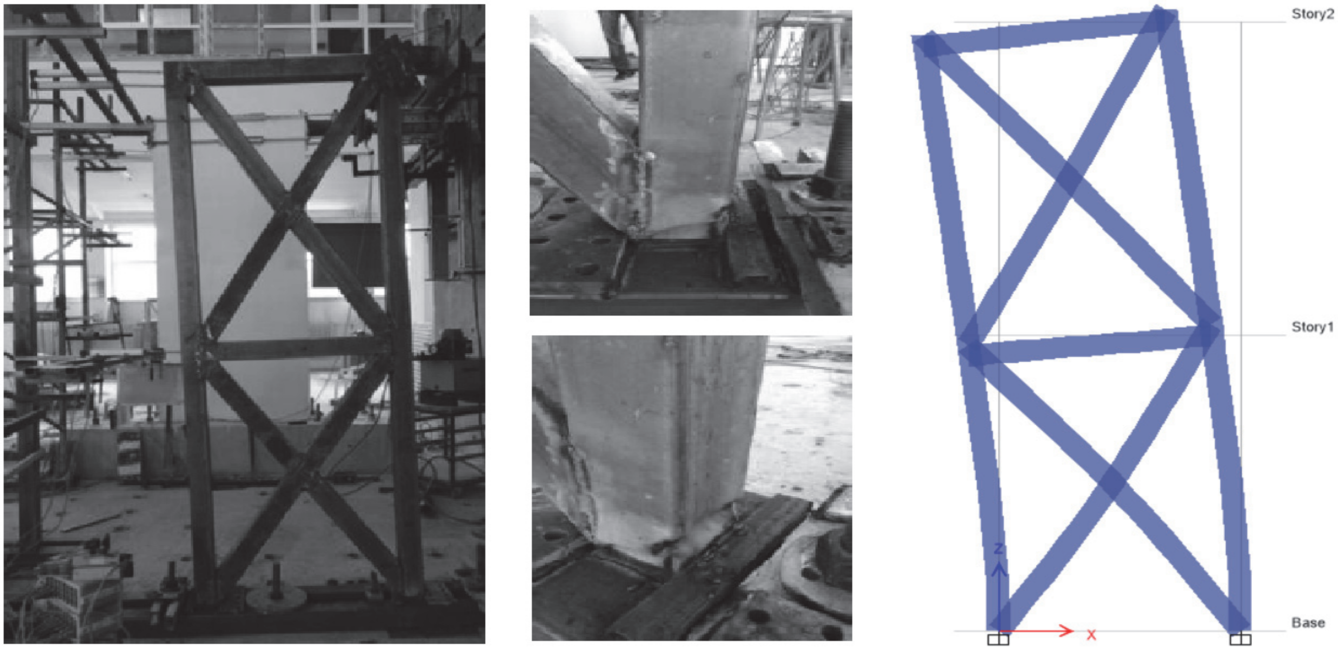

Figure 9: Damage under lateral load as measured experimentally [49] and predicted by ETABS.

FINDINGS ON CONTROLLED-STEEL BUILDINGS

Since this research aims to assess the earthquake resistance of a steel multi-story structure equipped with an eccentric X-brace, the findings must be as consistent as possible. The X-brace section of the control steel structures is W6 x 16 inches, and the buildings range in height from 6 to 12 stories. Tabs. 5 show the numerical outcomes of the W6x16 X-brace sectioned multi-story buildings (6, 9, and 12). The behavior of lateral displacements and lateral drift due to seismic stress is shown in Figs. 10 through 12 as a function of the eccentricity of the X-brace.

X-brace position	Building code	Eccentricity (mm)	e/L	Displacement X-direction (mm)	Increasing %	Displacement Y-direction (mm)	Increasing %	Max. Drift X-direction	Increasing %	Max. Drift Y-direction	Increasing %
Corner	**SC6-B16-1**	0	0	171.5	-	88.2	-	0.016	-	0.006	-
	SC6-B16-2	500	0.094	197.2	14.9	99.6	12.9	0.017	6.3	0.007	16.7
	SC6-B16-3	1000	0.188	316.9	84.7	158.2	58.8	0.023	43.8	0.010	66.7
	SC6-B16-4	1500	0.282	375.8	119.1	159.4	0.8	0.028	75.0	0.011	83.3
Side	**SS6-B16-1**	0	0	158.9	-	78.8	-	0.015	-	0.006	-
	SS6-B16-2	500	0.094	196.7	23.8	110.5	40.2	0.017	13.3	0.008	33.3
	SS6-B16-3	1000	0.188	309.0	94.4	158.6	43.5	0.022	46.7	0.010	66.7
	SS6-B16-4	1500	0.282	367.4	131.2	159.4	0.5	0.027	80.0	0.011	83.3
Corner	**SC9-B16-1**	0	0	397.5	-	227.8	-	0.021	-	0.013	-
	SC9-B16-2	500	0.094	406.3	2.2	269.7	12.9	0.021	0	0.014	7.7
	SC9-B16-3	1000	0.188	482.0	21.3	354.4	79.4	0.023	9.5	0.018	38.5
	SC9-B16-4	1500	0.282	432.9	8.9	384.8	80.7	0.025	19.1	0.019	46.2
Side	**SS9-B16-1**	0	0	391.0	-	224.3	-	0.021	-	0.012	-
	SS9-B16-2	500	0.094	401.6	2.7	256.2	40.2	0.021	0	0.014	16.7
	SS9-B16-3	1000	0.188	491.6	25.7	331.6	101.3	0.023	9.5	0.018	50.0
	SS9-B16-4	1500	0.282	435.4	11.4	377.9	102.3	0.026	23.8	0.018	50.0
Corner	**SC12-B16-1**	0	0	484.7	-	380.4	-	0.020	-	0.015	-
	SC12-B16-2	500	0.094	467.1	-3.6	382.9	0.7	0.021	5.0	0.017	13.3
	SC12-B16-3	1000	0.188	406.9	-16.1	379.6	-0.2	0.019	-5.0	0.016	6.7
	SC12-B16-4	1500	0.282	388.0	-19.9	376.2	-1.1	0.021	5.0	0.015	0
Side	**SS12-B16-1**	0	0	474.0	-	400.0	-	0.020	-	0.014	-
	SS12-B16-2	500	0.094	464.4	-2.0	372.4	-6.9	0.020	0	0.015	7.2
	SS12-B16-3	1000	0.188	409.0	-13.7	360.5	-9.9	0.019	-5.0	0.016	14.3
	SS12-B16-4	1500	0.282	389.2	-17.9	369.6	-7.6	0.020	0	0.015	7.2

Table 5: Numerical results of the 6, 9 and 12-story buildings with X-brace with section of W6x16.

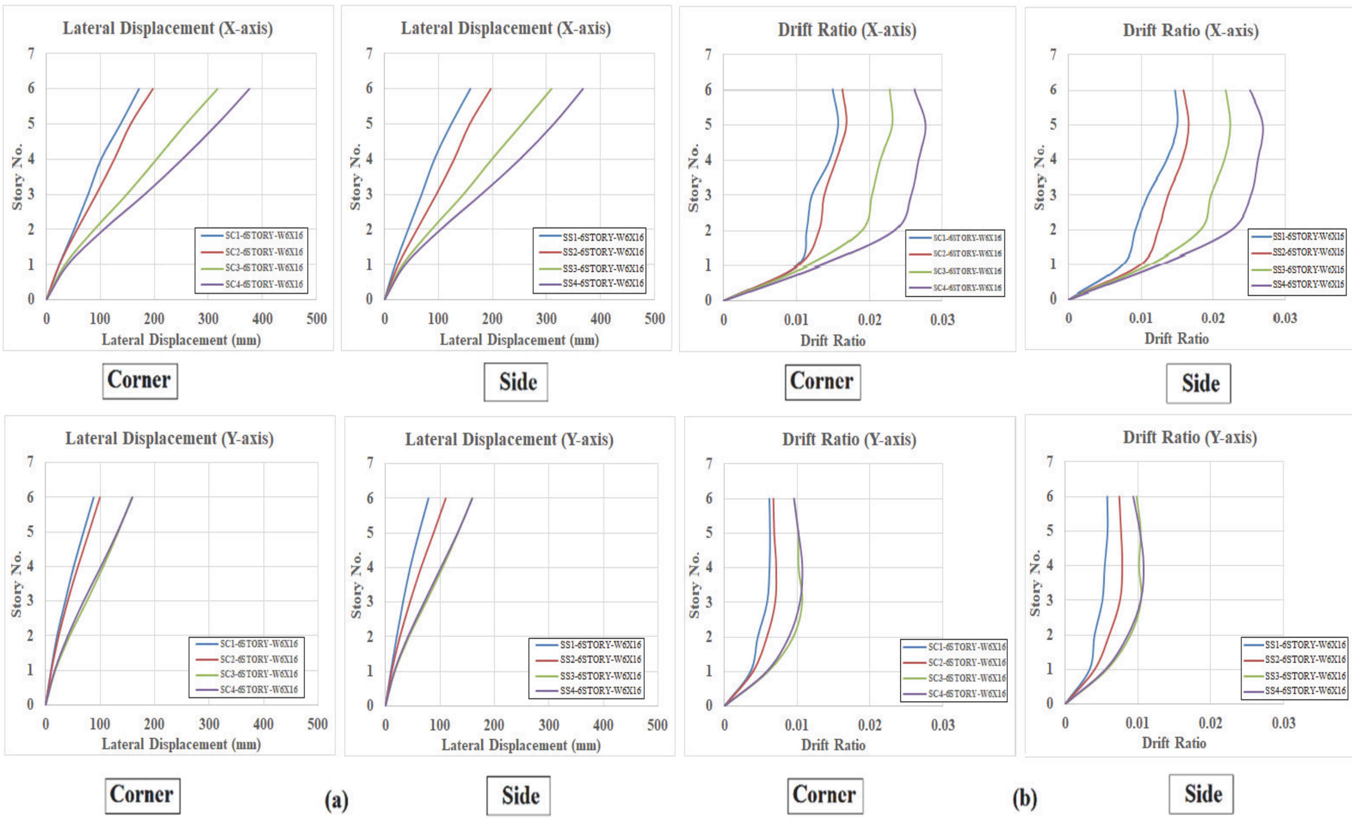

Figure 10: The 6-story buildings behavior (a) Story - lateral displacement curves and (b) Story -lateral drift curves.

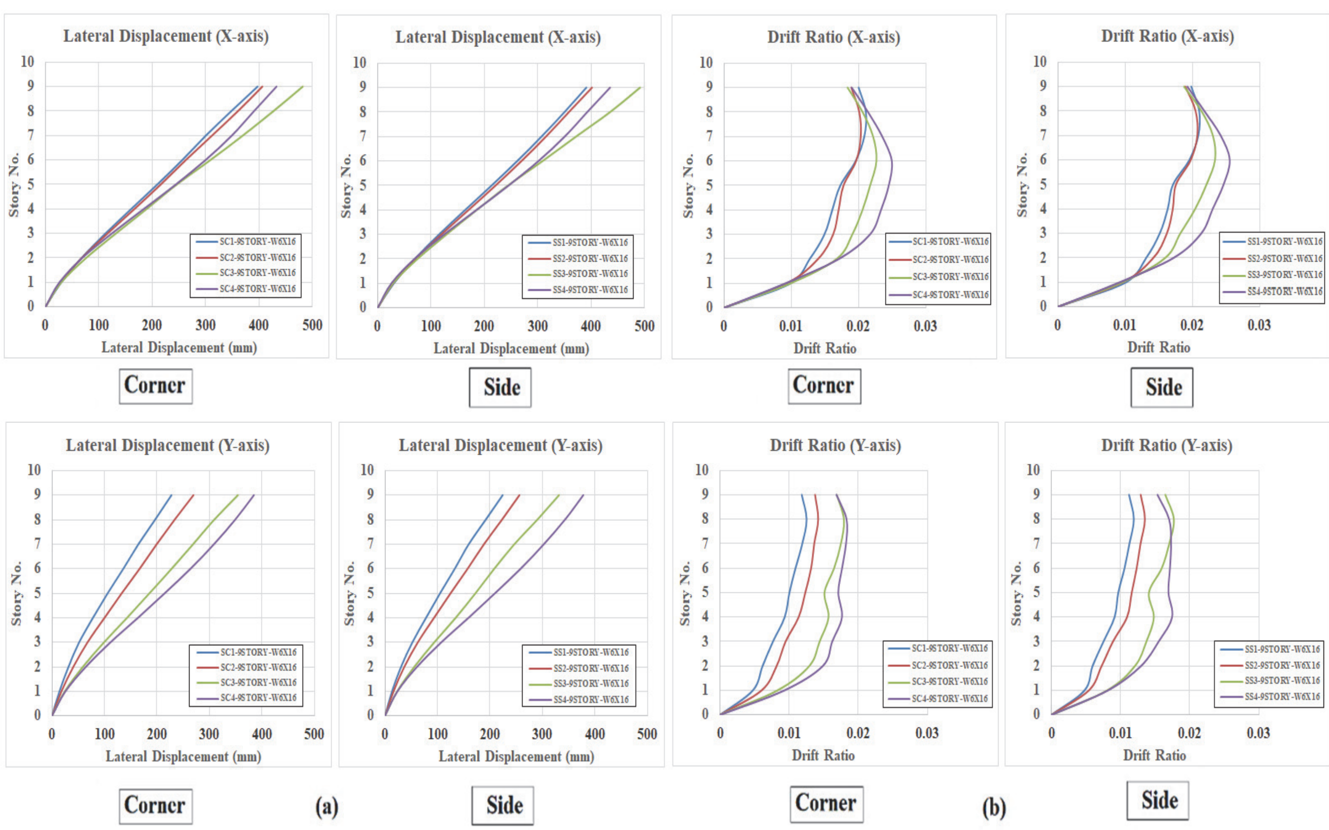

Figure 11: The 9-story buildings behavior (a) Story - lateral displacement curves and (b) Story -lateral drift curves.

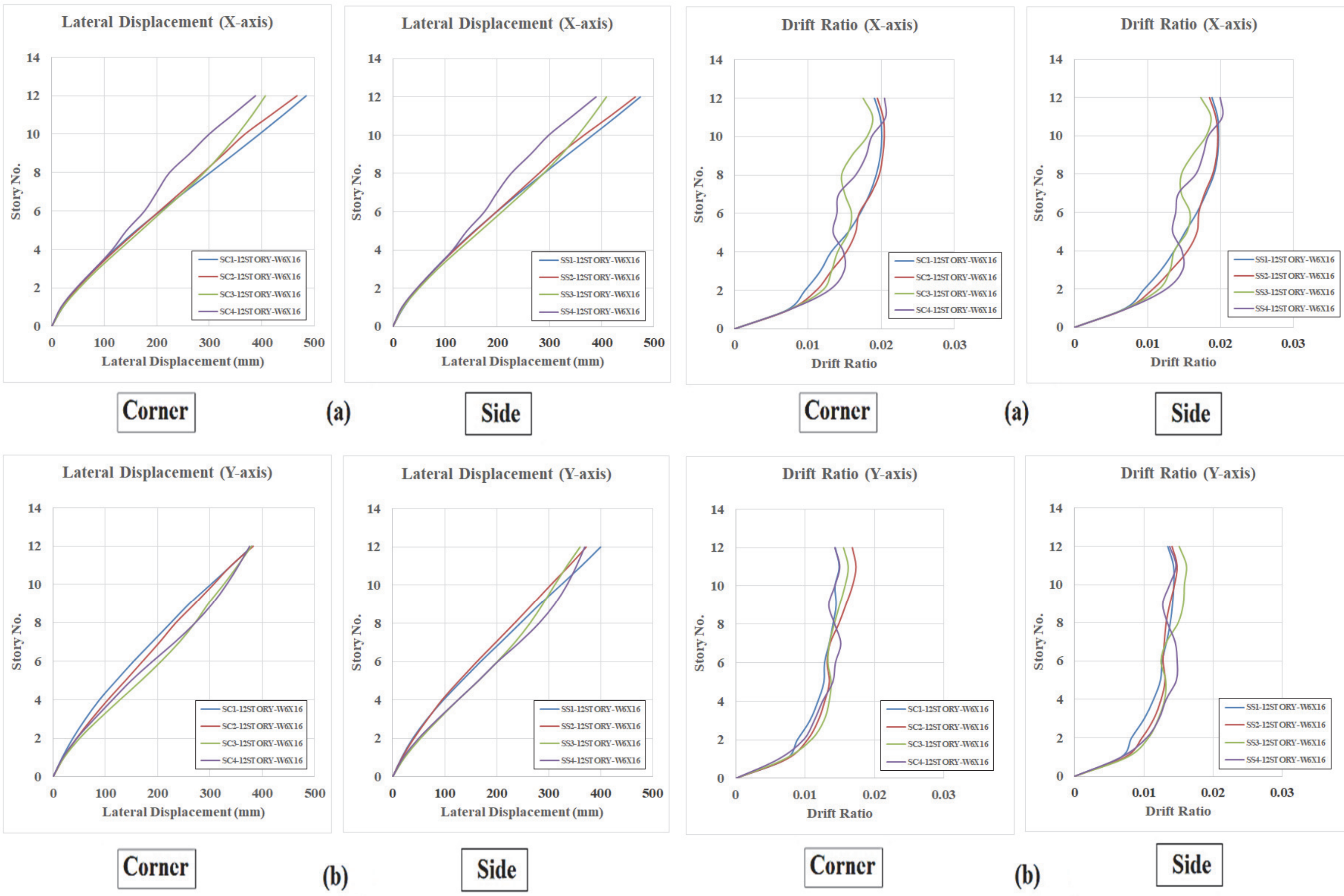

Figure 12: The 12-story buildings behavior (a) Story - lateral displacement curves and (b) Story -lateral drift curves.

Effect of eccentric X-bracing on the story lateral displacement

The impact of bracings may be studied using story lateral displacement tables and graphs. It is found that the lateral displacements at each story level may be significantly increased at the top story level by adding different eccentric bracing patterns to the basic frame structure. The chart shows that for multi-story buildings with six stories and an X-brace section of W6x16 at the corner position, the lateral displacement rises by 14.9%, 84.7%, and 119.1% as eccentricity increases. Moreover, for multi-story buildings with a W6x16 eccentric X-brace section at the side position, an increased eccentrically braced frame increased lateral displacement by 23.8%, 94.4%, and 131.2%.

For 9-story multi-story buildings with an X-brace section of W6x16 in the corner position, increasing the eccentricity of the bracing from 0 to 1500mm increased the lateral displacement of by 12.9 percent, 79.4 percent and 80.7 percent, respectively. Furthermore, for multi-story buildings with an X-brace section of W6x16 at the side position, increases in eccentrically braced frames from 0 to 1500mm resulted in increasing the lateral displacement of by 40.2, 101.3 and 102.3 percent, respectively. For 12-story multi-story buildings with an X-brace section of W6x16 at the corner site, the lateral displacement decreased by 3.6%, 16.1%, and 19.9% as the eccentricity of the bracing increased. Furthermore, for multi-story buildings with a W6x16 eccentric X-brace section at the side position, the lateral displacement decreased by 2.0%, 13.7%, and 17.9% as stories increased.

Compared to 9- and 12-story multi-story structures, the findings show that eccentric X-braces are superior at minimizing upper-story displacement in 6-story multi-story buildings. Lateral displacement at each floor rose as the eccentricity of the eccentric X-brace did since the structure became less stiff laterally.

Effect of eccentric X-bracing on the story drift

Tables and figures in story lateral drift format may be used to study the impact of bracings. Different eccentric bracing patterns are added to the basic frame structure, improving lateral displacements at each story level and significantly increasing the displacement at the top story level. The chart shows that the lateral drift of 6-story multi-story buildings with an X-brace section of W6x16 at the corner increased by 16.7%, 66.7%, and 83.3% when eccentric bracing was added to the frame. Furthermore, for 6-story multi-story buildings with an X-brace section of W6x16 in the side position, an increased eccentrically braced frame increased lateral drift by 33.3%, 66.7%, and 83.3%.

For 9-story multi-story buildings with an X-brace section of W6x16 at the corner position, the maximum lateral drift was increased by 7.7%, 38.5% and 46.2%, respectively, when the eccentricity of the frame was raised from 0 to 1500mm. For 9-story multi-story buildings with an X-brace section of W6x16 at the side position, the maximum lateral drift was increased by 16.7, 50 and 50 %, respectively, for increases in eccentrically braced frames from 0 to 1500mm. The maximum lateral drift for 12-story multi-story buildings with a W6x16 X-brace section at the corner increased by 13.3%, 6.7%, and 5% when the eccentric bracing of the frame was increased. Also, for multi-story buildings with 12 stories and an X-brace section of W6x16 in the side position, the lateral drift increased by 7.2%, 14.3%, and 7.2% as the eccentricity of the bracing increased. Based on the data, eccentric X-braces are better suited for six-story buildings than nine- or twelve-story buildings to avoid story drift. When designing a building with six stories, increasing the eccentricity of the X-brace reduces the lateral stiffness of the structure, causing a more significant lateral displacement on each floor. Buildings with nine and twelve stories have improved the basic frame structure's lateral stiffness, reducing story displacements and, consequently, deviations at each level. The previous figures show that eccentric X-braces are stiffer than concentrically supported edges. So, displacement, drift, relatively increased, and base shear will all be magnified in a system with eccentric bracing. Lateral height drift is more pronounced between eccentric X-brace and other lower-level supports. As a result of their low horizontal rigidity, eccentric X-braces can provide more structural variation than concentrically supported edges. Due to a reduction in the earthquake's effect with altitude, inter-story drift is reduced. Compared to eccentric X-braces, the lateral stiffness of edges braced using concentric X-braces is the greatest.

Effect of eccentricity of X-brace on the seismic behavior

One can examine its maximal base shear to demonstrate how much force an earthquake may exert on a structure's foundation. Tab. 6 displays the maximum allowable lateral displacement, drift, and base shear for the X-braced control steel structure models. Figs. 13 through 15 depict the compression of the maximal base shear generated at the foundation of each steel building model subjected to applied seismic pressures. Figs. 16–18 show how the base shear changes over time for 6-story, 9-story, and 12-story buildings with W6x16 X-brace sections in the corners. Figs. 19–21 show how the time hysteresis of base shear changes for buildings with six, nine, or twelve stories and a W6x16 eccentric X-brace in the side position.

No. of Story	X-brace position (Corner)						X-brace position (Side)					
	Eccentricity (mm)	Building ID	Δu max (mm)	Drift max (mm/mm)	Base shear Vmax (kN)	Maximum Brace force (kN)	Eccentricity (mm)	Building ID	Δu max (mm)	Drift max (mm/mm)	Base shear Vmax (kN)	Maximum Brace force (kN)
6	0	**SC6-B16-1**	171.5	0.0157	11354.5	1657.8	0	**SS6-B16-1**	158.9	0.0151	9918.9	1401.8
	500	**SC6-B16-2**	197.2	0.0168	11197.2	2137.9	500	**SS6-B16-2**	196.7	0.0166	11146.2	2043.9
	1000	**SC6-B16-3**	316.9	0.0231	8451.4	2411.9	1000	**SS6-B16-3**	309.1	0.0216	8321.9	2286.7
	1500	**SC6-B16-4**	375.8	0.0276	7042.7	2783.1	1500	**SS6-B16-4**	367.4	0.0269	6962.9	2674.1
9	0	**SC9-B16-1**	397.5	0.0211	10805.8	1596.2	0	**SS9-B16-1**	391.0	0.0210	10705.3	1530.9
	500	**SC9-B16-2**	406.3	0.0203	9601.1	1887.6	500	**SS9-B16-2**	401.6	0.0207	9799.0	1825.0
	1000	**SC9-B16-3**	482.1	0.0227	6910.3	2276.6	1000	**SS9-B16-3**	491.6	0.0233	6738.1	1916.7
	1500	**SC9-B16-4**	432.9	0.0249	4751.2	2388.4	1500	**SS9-B16-4**	435.4	0.0255	4832.8	1916.8
12	0	**SC12-B16-1**	484.7	0.0201	7586.2	1467.4	0	**SS12-B16-1**	474.0	0.0197	7185.0	1052.8
	500	**SC12-B16-2**	467.1	0.0204	7571.1	1828.7	500	**SS12-B16-2**	464.4	0.0196	7311.1	1460.8
	1000	**SC12-B16-3**	406.9	0.0188	5346.9	1731.3	1000	**SS12-B16-3**	409.1	0.0187	5264.5	1642.3
	1500	**SC12-B16-4**	388.0	0.0206	4152.9	1736.4	1500	**SS12-B16-4**	389.2	0.0203	4260.3	1716.3

Table 6: Numerical results of the 6, 9 and 12-story buildings with X-brace with section of W6x16.

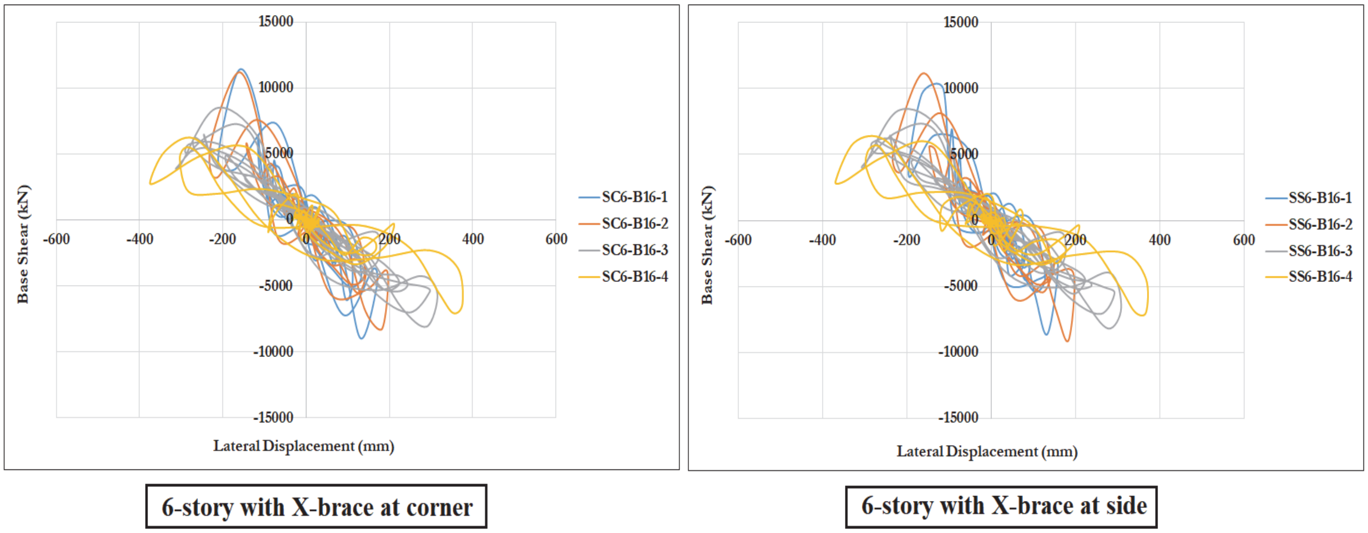

Figure 13: Base shear-lateral displacement curve of the 6-story buildings

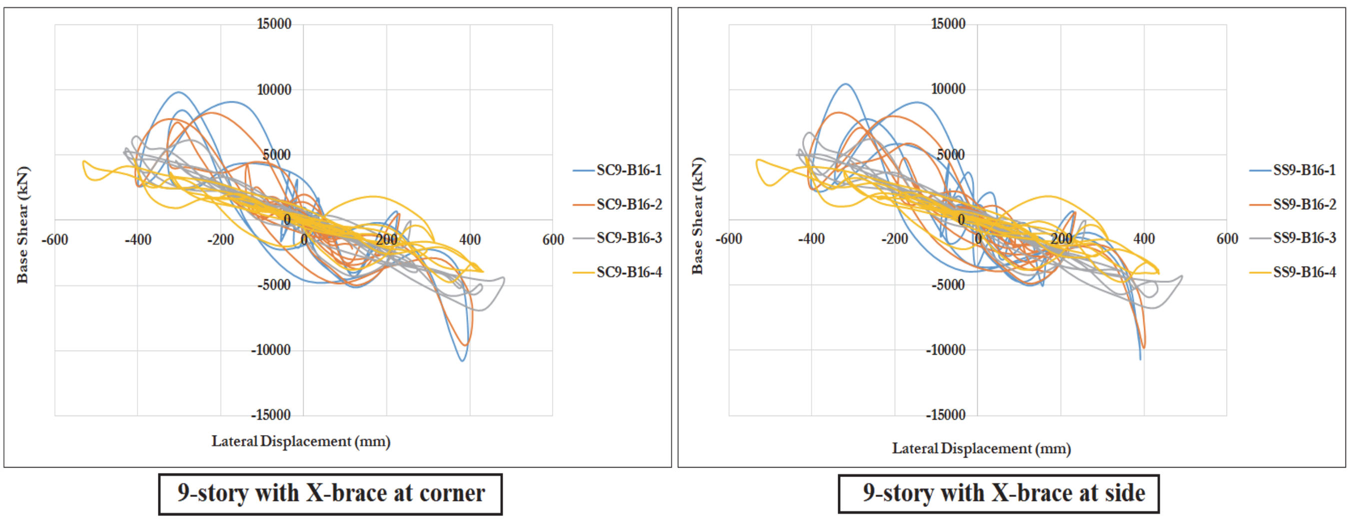

Figure 14: Base shear-lateral displacement curve of the 9-story buildings.

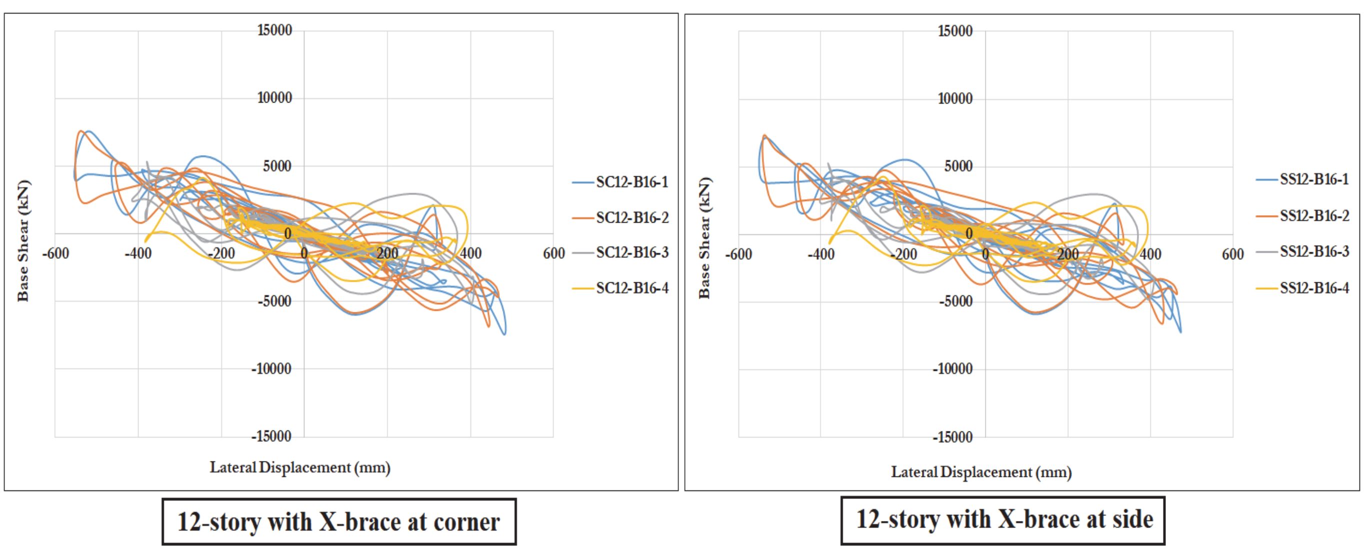

Figure 15: Base shear-lateral displacement curve of the 12-story buildings.

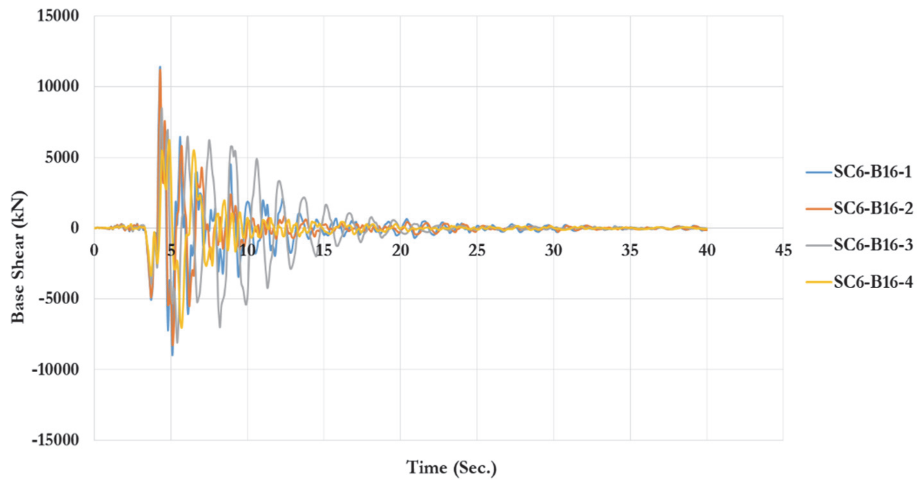

Figure 16: Comparison of time hysteresis of base shear for different cases of the 6-story buildings with X-brace section of W6x16 at corner position.

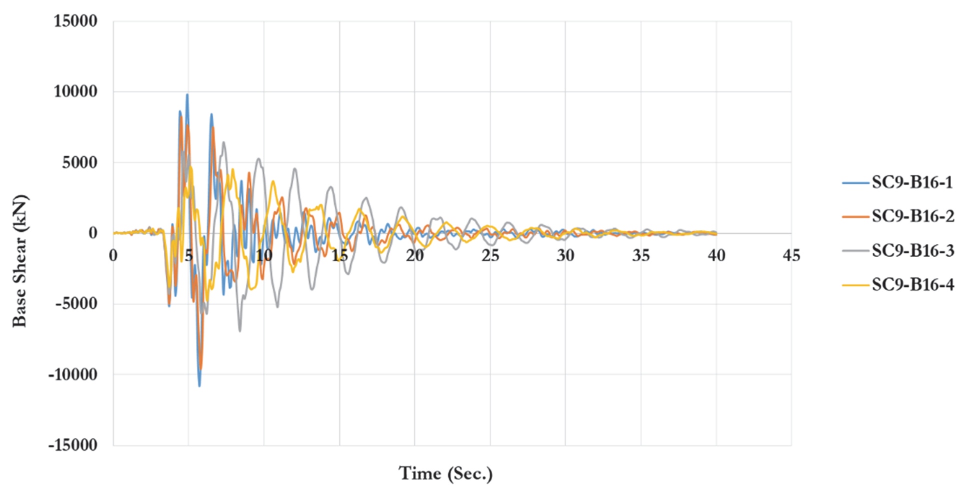

Figure 17: Comparison of time hysteresis of base shear for different cases of the 9-story buildings with X-brace section of W6x16 at corner position.

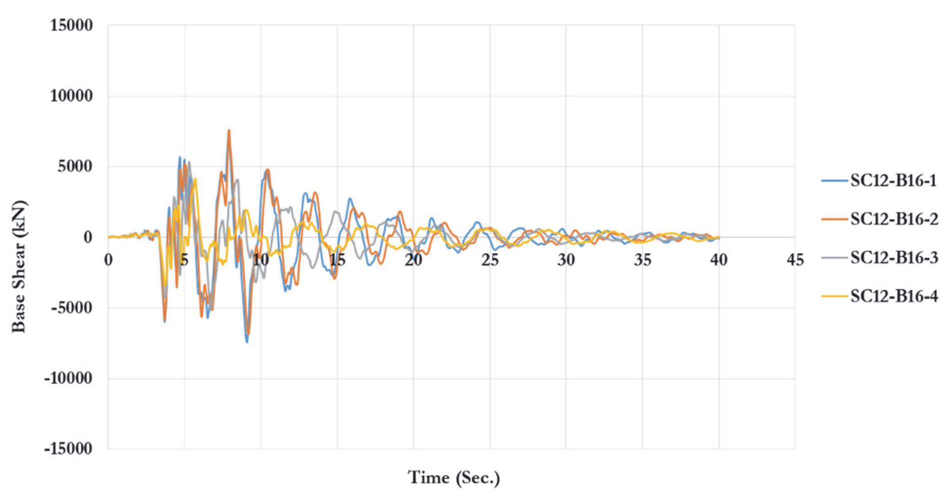

Figure 18: Comparison of time hysteresis of base shear for different cases of the 12-story buildings with X-brace section of W6x16 at corner position.

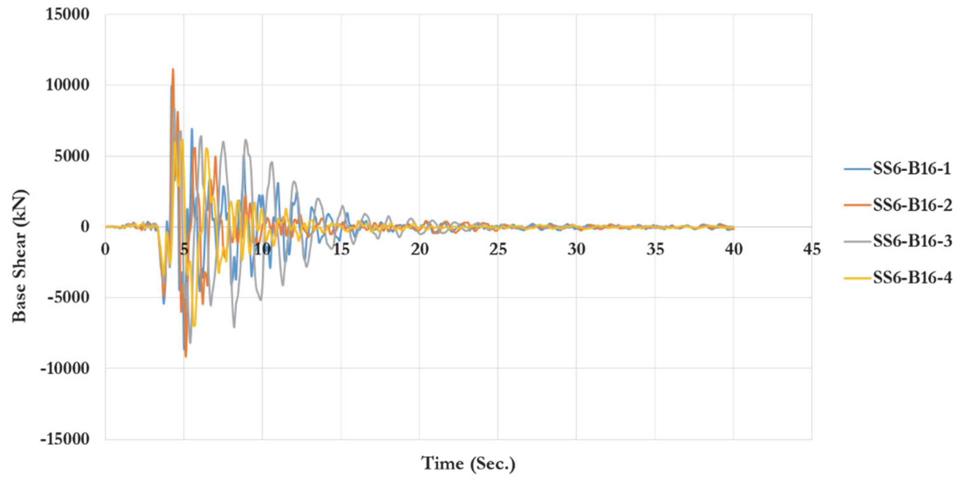

Figure 19: Comparison of time hysteresis of base shear for different cases of the 6-story buildings with X-brace section of W6x16 at side position.

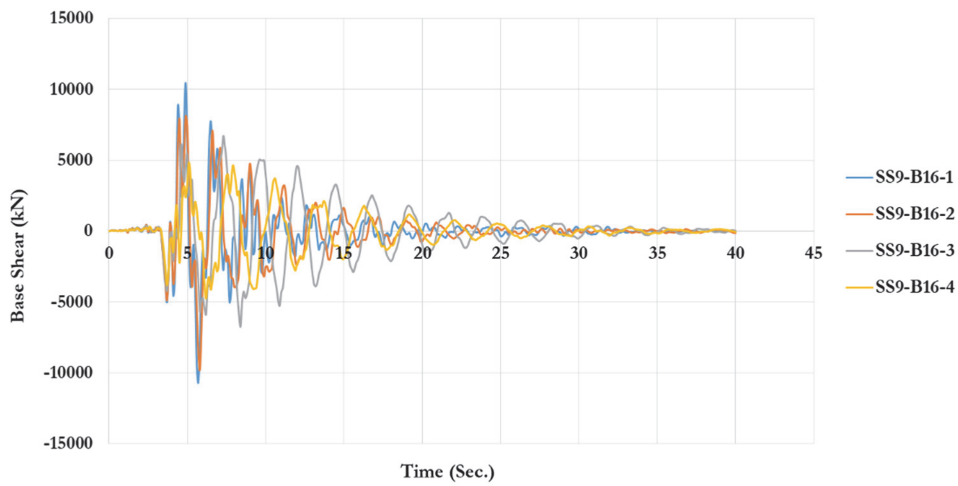

Figure 20: Comparison of time hysteresis of base shear for different cases of the 9-story buildings with X-brace section of W6x16 at side position.

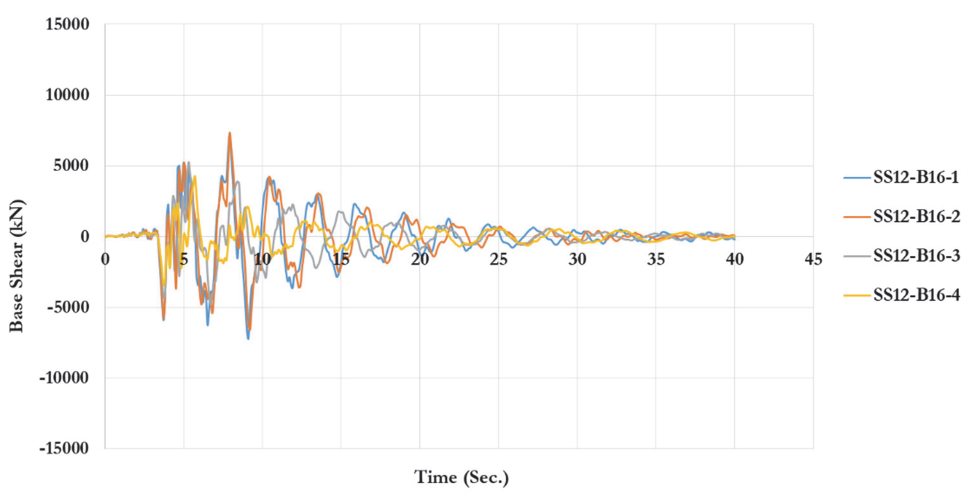

Figure 21: Comparison of time hysteresis of base shear for different cases of the 12-story buildings with X-brace section of W6x16 at side position.

The influence of eccentricity on X-bracings may be studied with base shear (Vmax) and maximum brace force tables and figures. For 6-story structures with an X-brace section of W6x16 at the corner position had a 1.38%, 25.57% and 37.97%, respectively reduced in base shear as the eccentricity of the bracing frame increased from 0 to 1500mm. Also, for multi-story buildings with a 6-story height and an X-brace section of W6x16 in the side position, an increase in eccentrically braced frames resulted in a decrease in base shear of 1.83 percent, 26.71 percent, and 38.67 percent, respectively.
Multi-story buildings with 9 stories with an X-brace section of W6x16 at the corner position saw an increase in eccentrically braced frames decrease base shear by 11.14%, 36.05%, and 56.03%. Also, for 9-story multi-story buildings with X-brace section W6x16 at side position, an increase in eccentrically braced frames from 0 to 1500mm resulted in decrease base shear by 9.31%, 37.64%, and 55.27%. For multi-story buildings with 12 stories and an X-brace section of W6x16 at the corner, the eccentrically braced frame resulted in a 0.19 percent, 29.52 percent, and 45.26 percent decrease in base shear. In addition, for 12-story multi-story buildings with an X-brace section of W6x16 in the side position, an increase in eccentrically braced frames decreased base shear by 3.63%, 30.61%, and 43.84%.
For 6-story structures with an X-brace section of W6x16 at the corner position had a 28.96%, 45.49% and 67.88%, respectively increased in brace force as the eccentricity of the bracing frame increased from 0 to 1500mm. Also, for multi-story buildings with a 6-story height and an X-brace section of W6x16 in the side position, an increase in eccentrically braced frames resulted in an increased in brace force of 23.28 percent, 37.94 percent, and 61.30 percent, respectively.
Multi-story buildings with 9 stories with an X-brace section of W6x16 at the corner position saw an increase in eccentrically braced frames increased brace force by 18.26%, 42.63%, and 49.63%. Also, for 9-story multi-story buildings with X-brace section W6x16 at side position, an increase in eccentrically braced frames from 0 to 1500mm resulted in increased brace force by 14.33%, 20.07%, and 20.09%. For multi-story buildings with 12 stories and an X-brace section of W6x16 at the corner, the eccentrically braced frame resulted in a 24.62 percent, 17.98 percent, and 18.33 percent increase in brace force. In addition, for 12-story multi-story buildings with an X-brace section of W6x16 in the side position, an increase in eccentrically braced frames changed in brace force by – 0.45%, 11.92%, and 16.96%.
Eccentric X-braces decrease brace force in six-story multi-story buildings more than nine- or twelve-story ones. The X-brace force increased as eccentricity lowered lateral stiffness. The eccentricity of the X-brace decreases the structure's lateral stiffness, boosting steel frame ductility and minimizing base shear hysteresis. Figs. 13–15 show that the eccentric X-brace bends faster along a wall than at a corner. Low-rise frames dissipate more energy, proving the eccentric X-brace works better. Eccentricity influenced the braced frame's strength, stability, and ductility since the horizontal links' length indicated the system's energy dissipation capacity. Short links (little eccentricity) rapidly affect shear in the connections, whereas longer links (large eccentricity) may bend. Shorter linkages (small eccentricities) improve shear-yielding efficiency.
Otherwise, more eccentricity increases flexural yielding, whereas shorter connections with less eccentricity increase shear yielding. Eccentric braces are more flexible. Thus, their lateral rigidity is lower than that of concentrically braced frames, particularly diagonally braced ones. Eccentric braces delay the building's reaction to an earthquake, giving residents more time to leave, while structural bracing reduces ground vibrations. Eccentrically braced frames last longer and are the most versatile. Eccentric X-braces are flexible but less rigid than concentrically braced frames. Eccentric X-braces have excellent ductility but low lateral stiffness, making seismic design difficult. The numerical method correctly estimates lateral displacement, maximum drift, and base shear. It matches Abolfazl and Imanpour [52], Tian et al. [53] and Wang et al. [54].

EFFECT OF THE CHANGING IN X-BRACE SECTION ON THE BEHAVIOR OF BUILDINGS

This part will examine how modifying the X-brace section influences the building assembly. The X-brace included H-shaped diagonals. Five steel sections were chosen for the X-brace (W-6x12, W-6x15, W-6x16, W-6x20, and W-6x25), and a multi-story steel structure using the W6x16 X-brace section was used as a control. Maximum lateral displacement, drift, and base shear for the X-brace steel section (W-6x12, W-6x15, W-6x16, W-6x20, and W-6x25) at corner and side positions are shown in Tabs. 7–9. The story-lateral drift of the 6-story buildings with varying X-brace sections at the corner and side locations is also shown in Fig. 22. The 9-story buildings with corner and side X-brace sections of various kinds demonstrate lateral drift in Fig. 23. The twelve-story structures with various eccentric X-brace sections in the corners and sides are seen drifting laterally in Fig. 24.
The effects of altering the eccentric X-brace section may be analyzed using horizontal movement charts and tables. There is a 17.76% rise in lateral story displacement for buildings with six stories with corner X-braces when the X-brace section is reduced from W-6x16 to W-6x12 and an 18.02% decrease when the X-brace section is reduced from W-6x16 to W-6x25. When the eccentricity was 500 mm, the results were an increase of 16.27 percent and a drop of 16.02 percent with a smaller X-brace section. When the eccentricity was 1000 mm, the results were an increase of 6.5 percent and a decrease of 13.0

percent, respectively. Reduced by 5.85% but increased by 3.0%, the X-brace portion was used when the eccentricity was 1500 mm. The lateral drift of the story rise by 14.01%, 17.85%, and 5.62% when the eccentricity was modified from 0 to 1000 mm and dropped by 15.92%, 5.35%, and 2.16% when the X-brace section was changed. The X-brace cross-section decreased by 0.72% but increased by 1.08% with an eccentricity of 1500 mm.

Story lateral displacement increased by 10.69%, 14.18%, and 5.43% and decreased by 18.75%, 15.81%, and 11.9% for 6-story buildings with eccentric X-braces at side positions. To achieve an eccentricity of 1500 mm, a reduction of 4.24% and an increase of 5.4% were applied to the X-brace section. The lateral drift of the story increased by 5.96%, 18.67%, and 0% when the eccentricity varied from 0 to 1000 mm and decreased by 26.49%, 0%, and 10.18% when the eccentricity varied from 0 to 1000 mm due to changes in the X-braces section. For an eccentricity of 1500 mm, we saw a decrease in the X-brace area of 1.86% and 3.72%.

For the buildings with nine stories with corner X-braces, the story lateral displacement was found to shift by 4.5 percentage points, 2.65 percentage points, 6.67 percentage points, and -3.8 percentage points when the X-brace section was decreased, and by -3.8 percentage points, -4.4 percentage points, -11.4 percentage points, and 12.05% when the X-brace section was raised, all with increasing eccentricity. When the X-brace section was lowered, the story lateral drift changed by -4.73%, 1.48%, 3.94%, and -4%; when it was elevated, the numbers were 4.73%, 2.96%, -10.57%, and 1.61%. A reduction in the X-brace section reduces the lateral displacement of the story by 4.65%, 3.18%, 4.39%, and -3.3% as eccentricity rises. In contrast, an increase in the X-brace section reduces the lateral displacement by 1.99%, -1.72%, -9.9%, and 9.07%. Additional variations in the story lateral drift of -5.23%, 0.48%, 1.72%, and -6.3% were caused by reducing the size of the X-brace, whereas increases of 4.3%, 2.89%, -8.58%, and -0.4% were caused by increasing the section of the eccentric X-brace.

For the buildings with twelve stories with corner X-braces, the story lateral displacement was found to decrease by 2.99%, 0.41%, 0.88%, and 0.15% when the X-brace section was reduced, 6.5%, 4.75%, 6.43%, and 1.67% when the X-brace section was raised, and by 2.48%, - 0.49%, 0%, and 0.97% when the eccentricity was increased. Additionally, changes in the story lateral drift of 3.98%, 0%, -4.25%, and -6.79% were caused by reducing the size of the X-brace, whereas changes of -1.11%, 0.25%, -2.51% and -0.61% were caused by increasing the section of the X-brace, respectively. For decreasing and increasing X-brace sections with increasing eccentricity, lateral story displacement decreased by 7.81%, 1.11%, 6.5%, and 1.69%, respectively. Alterations in the story lateral drift of 1.52%, 0.51%, -1.07%, and 1.48% were also seen for X-brace sizes decreasing from large to small and of 3.56%, 1.02%, -4.27%, and -4.93% for eccentric X-brace sizes rising.

	X-brace position (Corner)						X-brace position (Side)					
No. of Story	Eccentricity (mm)	Building ID	Δu max (mm)	Drift max (mm/mm)	Vmax (kN)	Maximum Brace force (kN)	Eccentricity (mm)	Building ID	Δu max (mm)	Drift max (mm/mm)	Vmax (kN)	Maximum Brace force (kN)
6	0	**SC6-B12-1**	201.8	0.0179	11354.6	1640.3	0	**SS6-B12-1**	175.9	0.0160	11257.4	1590.2
		SC6-B15-1	181.9	0.0157	11504.9	1676.4		**SS6-B15-1**	162.9	0.0150	10166.4	1442.3
		SC6-B16-1	171.5	0.0157	11354.5	1657.8		**SS6-B16-1**	158.9	0.0151	9918.9	1401.8
		SC6-B20-1	160.9	0.0150	10453.9	1552.1		**SS6-B20-1**	142.8	0.0130	10698.8	1515.0
		SC6-B25-1	140.6	0.0132	10728.8	1567.9		**SS6-B25-1**	129.1	0.0111	10658.6	1512.3
	500	**SC6-B12-2**	229.3	0.0198	10628.6	1931.4	500	**SS6-B12-2**	224.6	0.0197	10774.4	1900.7
		SC6-B15-2	199.2	0.0177	11138.7	2102.2		**SS6-B15-2**	199.4	0.0175	11153.6	2028.5
		SC6-B16-2	197.2	0.0168	11197.2	2137.9		**SS6-B16-2**	196.7	0.0166	11146.2	2043.9
		SC6-B20-2	180.7	0.0161	11043.8	2190.2		**SS6-B20-2**	181.1	0.0169	10876.3	2048.9
		SC6-B25-2	165.6	0.0159	10562.6	2182.9		**SS6-B25-2**	165.6	0.0166	10067.1	1954.4
	1000	**SC6-B12-3**	337.5	0.0244	7925.4	2120.2	1000	**SS6-B12-3**	325.9	0.0242	8199.2	2104.0
		SC6-B15-3	322.3	0.0238	8400.3	2358.7		**SS6-B15-3**	315.6	0.0231	8408.9	2255.6
		SC6-B16-3	316.9	0.0231	8451.4	2411.9		**SS6-B16-3**	309.1	0.0216	8321.9	2286.7
		SC6-B20-3	293.3	0.0230	8556.2	2493.2		**SS6-B20-3**	286.1	0.0235	8430.5	2409.2
		SC6-B25-3	275.7	0.0236	8889.2	2637.8		**SS6-B25-3**	272.2	0.0238	8921.7	2594.2
	1500	**SC6-B12-4**	387.1	0.0273	6354.9	2381.1	1500	**SS6-B12-4**	387.3	0.0274	6364.7	2306.7
		SC6-B15-4	381.0	0.0279	6852.0	2685.2		**SS6-B15-4**	373.3	0.0273	7042.8	2653.3
		SC6-B16-4	375.8	0.0276	7042.7	2783.1		**SS6-B16-4**	367.4	0.0269	6962.9	2674.1
		SC6-B20-4	362.7	0.0268	7669.2	3135.9		**SS6-B20-4**	359.6	0.0273	7824.8	3076.8
		SC6-B25-4	353.8	0.0278	8144.8	3229.0		**SS6-B25-4**	351.8	0.0279	8049.4	3290.2

Table 7: Numerical results for various X-brace sections of the 6-story buildings.

No. of Story	X-brace position (Corner)						X-brace position (Side)					
	Eccentricity (mm)	Building ID	Δu max (mm)	Drift max (mm/mm)	Vmax (kN)	Maximum Brace force (kN)	Eccentricity (mm)	Building ID	Δu max (mm)	Drift max (mm/mm)	Vmax (kN)	Maximum Brace force (kN)
9		**SC9-B12-1**	415.4	0.0201	8761.0	1299.7		**SS9-B12-1**	409.2	0.0199	9430.7	1347.3
		SC9-B15-1	402.4	0.0209	10288.4	1520.8		**SS9-B15-1**	393.3	0.0211	10501.4	1500.1
	0	**SC9-B16-1**	397.5	0.0211	10805.8	1596.2	0	**SS9-B16-1**	391.0	0.0210	10705.3	1530.9
		SC9-B20-1	382.1	0.0210	11813.2	1745.4		**SS9-B20-1**	396.2	0.0212	11468.4	1643.4
		SC9-B25-1	382.3	0.0221	12598.2	1879.8		**SS9-B25-1**	398.8	0.0219	13110.6	1880.1
		SC9-B12-2	417.1	0.0206	8042.1	1530.2		**SS9-B12-2**	414.4	0.0208	8628.8	1536.3
		SC9-B15-2	410.5	0.0202	9105.2	1783.7		**SS9-B15-2**	404.3	0.0203	9577.5	1766.7
	500	**SC9-B16-2**	406.3	0.0203	9601.1	1887.6	500	**SS9-B16-2**	401.6	0.0207	9799.0	1825.0
		SC9-B20-2	397.9	0.0211	10100.0	2043.5		**SS9-B20-2**	394.7	0.0212	10110.2	1938.9
		SC9-B25-2	388.3	0.0209	10535.0	2182.2		**SS9-B25-2**	394.7	0.0213	10457.4	2081.7
		SC9-B12-3	514.3	0.0236	6031.6	1813.0		**SS9-B12-3**	513.2	0.0237	5877.1	1577.0
		SC9-B15-3	493.3	0.0231	6781.9	2190.1		**SS9-B15-3**	499.3	0.0235	6664.6	1867.1
	1000	**SC9-B16-3**	482.1	0.0227	6910.3	2276.6	1000	**SS9-B16-3**	491.6	0.0233	6738.1	1916.7
		SC9-B20-3	456.3	0.0209	7004.6	2564.7		**SS9-B20-3**	471.5	0.0221	6784.6	2005.7
		SC9-B25-3	426.3	0.0203	7035.8	2754.7		**SS9-B25-3**	442.8	0.0213	7022.7	2201.1
		SC9-B12-4	416.3	0.0239	4800.8	2157.7		**SS9-B12-4**	420.9	0.0239	4822.3	1738.6
		SC9-B15-4	427.4	0.0241	4723.4	2365.3		**SS9-B15-4**	429.7	0.0249	4665.2	1835.5
	1500	**SC9-B16-4**	432.9	0.0249	4751.2	2388.4	1500	**SS9-B16-4**	435.4	0.0255	4832.8	1916.8
		SC9-B20-4	461.5	0.0253	4966.0	2464.3		**SS9-B20-4**	458.0	0.0252	4917.1	2136.8
		SC9-B25-4	485.1	0.0253	5696.5	2682.4		**SS9-B25-4**	474.9	0.0254	5848.2	2549.4

Table 8: Numerical results for various X-brace sections of the 9-story buildings.

No. of Story	X-brace position (Corner)						X-brace position (Side)					
	Eccentricity (mm)	Building ID	Δu max (mm)	Drift max (mm/mm)	Vmax (kN)	Maximum Brace force (kN)	Eccentricity (mm)	Building ID	Δu max (mm)	Drift max (mm/mm)	Vmax (kN)	Maximum Brace force (kN)
12		**SC12-B12-1**	470.2	0.0206	7132.8	1339.7		**SS12-B12-1**	468.7	0.0200	7453.2	1160.9
		SC12-B15-1	473.9	0.0201	7836.3	1467.7		**SS12-B15-1**	465.4	0.0194	7515.9	1098.4
	0	**SC12-B16-1**	484.7	0.0201	7586.2	1467.4	0	**SS12-B16-1**	474.0	0.0197	7185.0	1052.8
		SC12-B20-1	505.8	0.0209	7813.0	1517.7		**SS12-B20-1**	490.7	0.0206	8235.4	1205.1
		SC12-B25-1	516.2	0.0209	8103.7	1694.1		**SS12-B25-1**	511.0	0.0204	8225.9	1208.2
		SC12-B12-2	465.2	0.0203	6377.1	1624.3		**SS12-B12-2**	465.6	0.0197	5958.8	1340.2
		SC12-B15-2	469.9	0.0206	7317.4	1730.9		**SS12-B15-2**	467.2	0.0199	7159.9	1450.7
	500	**SC12-B16-2**	467.1	0.0204	7571.1	1828.7	500	**SS12-B16-2**	464.4	0.0196	7311.1	1460.8
		SC12-B20-2	468.7	0.0201	7647.2	2039.1		**SS12-B20-2**	468.6	0.0194	7381.0	1446.5
		SC12-B25-2	489.3	0.0204	7351.8	2147.5		**SS12-B25-2**	469.6	0.0198	6900.9	1391.7
		SC12-B12-3	403.3	0.0186	5228.3	1496.4		**SS12-B12-3**	398.8	0.0185	5294.0	1411.7
		SC12-B15-3	405.1	0.0188	5280.1	1620.0		**SS12-B15-3**	404.5	0.0187	5283.1	1567.7
	1000	**SC12-B16-3**	406.9	0.0188	5346.9	1731.3	1000	**SS12-B16-3**	409.1	0.0187	5264.5	1642.3
		SC12-B20-3	419.3	0.0186	5207.4	2106.2		**SS12-B20-3**	424.9	0.0185	5316.8	1882.1
		SC12-B25-3	433.1	0.0180	5861.3	2519.6		**SS12-B25-3**	435.7	0.0179	5796.0	2020.0
		SC12-B12-4	388.6	0.0208	3290.2	1349.8		**SS12-B12-4**	386.8	0.0206	3305.1	1342.8
		SC12-B15-4	386.2	0.0207	3890.1	1638.2		**SS12-B15-4**	387.4	0.0205	4079.4	1645.8
	1500	**SC12-B16-4**	388.0	0.0206	4152.9	1736.4	1500	**SS12-B16-4**	389.2	0.0203	4260.3	1716.3
		SC12-B20-4	392.3	0.0198	4559.2	2046.9		**SS12-B20-4**	393.4	0.0195	4770.2	2017.8
		SC12-B25-4	394.5	0.0192	4880.2	2316.6		**SS12-B25-4**	395.8	0.0193	5165.2	2234.8

Table 9: Numerical results for various X-brace sections of the 12-story buildings.

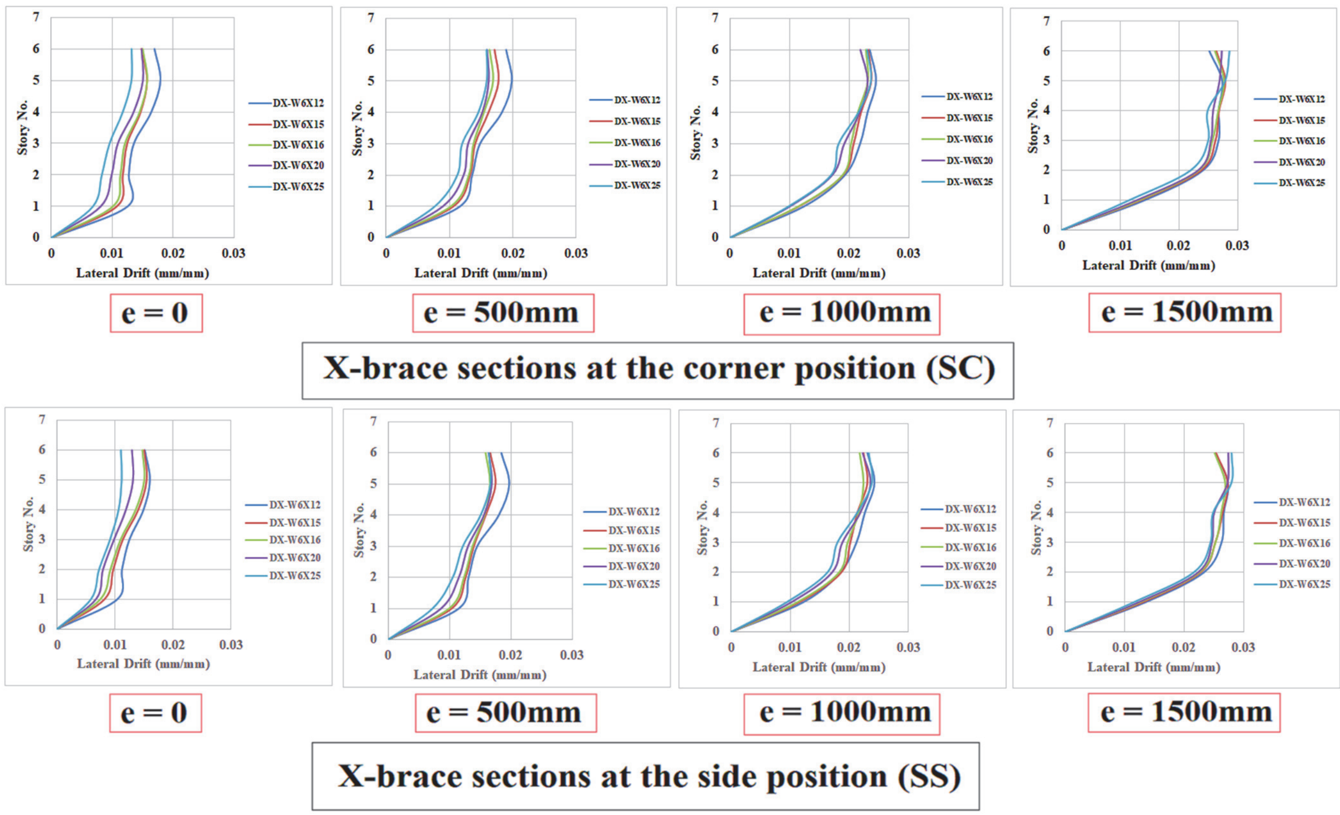

Figure 22: The story-lateral drift at x-directions of the 6-story buildings with the various types of X-brace sections at the corner and side positions.

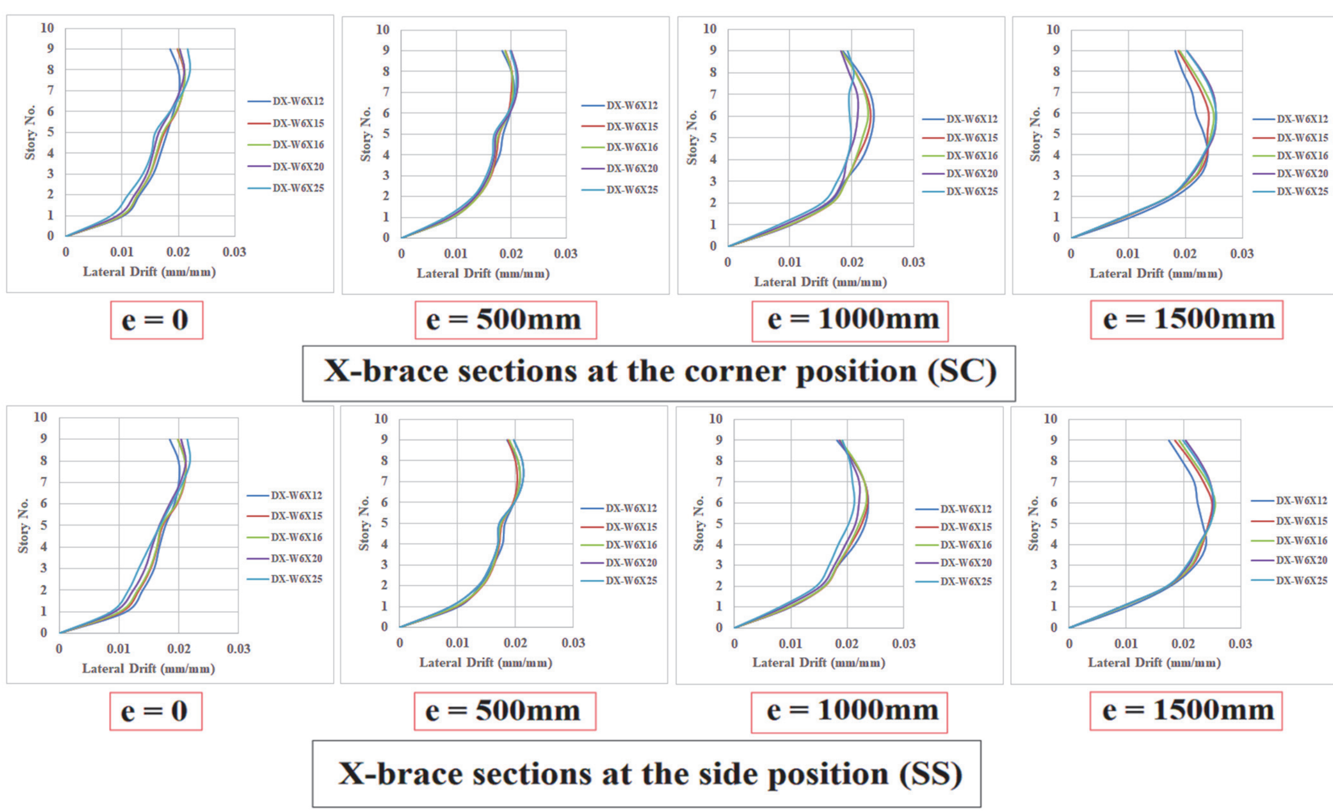

Figure 23: The story-lateral drift at y-directions of the 9-story buildings with the various types of X-brace sections at the corner and side positions.

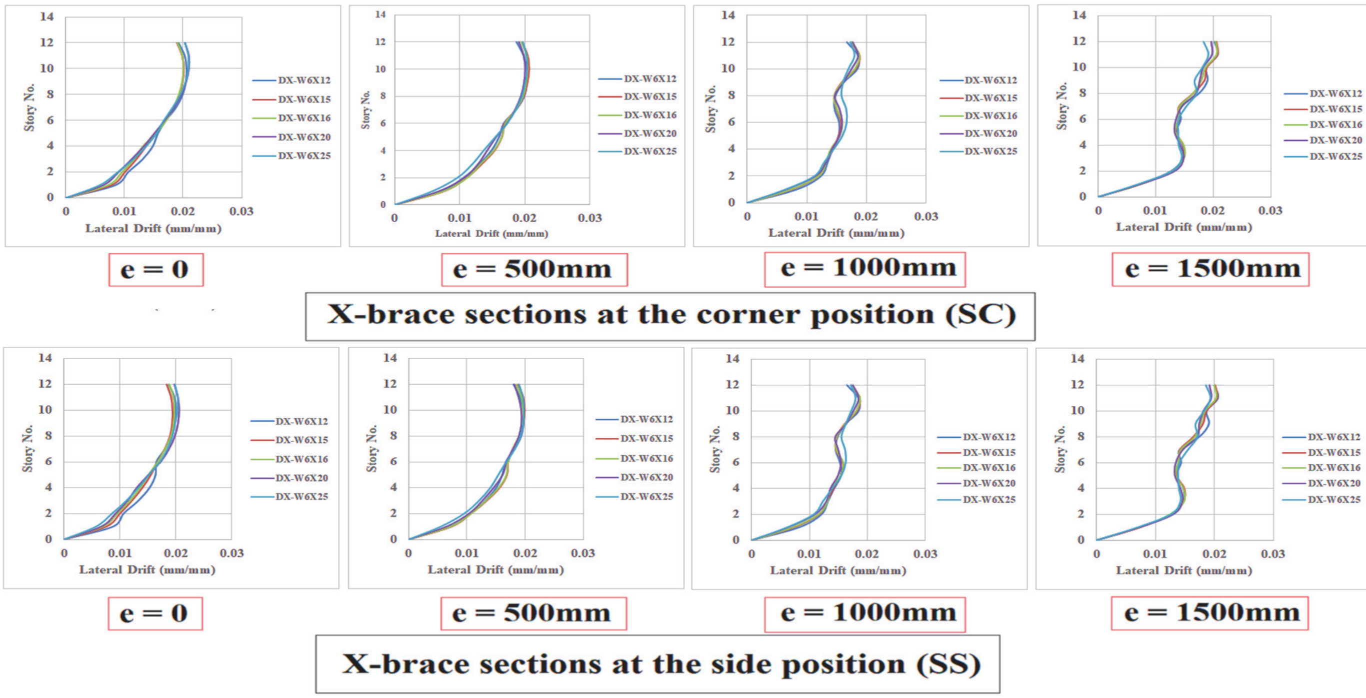

Figure 24: The story-lateral drift at y-directions of the 12-story buildings with the various types of X-brace sections at the corner and side positions.

When the eccentric X-brace is at a corner position, modifying its section is most successful in reducing the brace force for 6-story multi-story structures, as opposed to 9- and 12-story multi-story buildings. Large sections are required for eccentric X-braces to resist earthquake stresses, which drives up the cost of the materials used compared to bracing structures, reducing section size. The study results may show the X-bracing system's ability to strengthen the building's stiffness and minimize displacement. To compensate for eccentricity's effect on rigidity loss, expanding the X-braced member's cross-section may help. Moreover, the horizontal movement of eccentric X-braces is more significant. The ductility of the eccentric brace frame varies greatly depending on the X-brace section and eccentricity since an eccentric X-brace can absorb tremendous energy.

Height, eccentricity, section size, and the position of the X-brace in steel all influence the frequency with which an architectural design arises in nature. Natural frequency and period of all buildings is shown in Tabs. 10 and 11. A structure's natural frequency is more significant at lower heights and decreases with increasing eccentricity and increases the section size. Because the side position is more flexible, the natural frequency of a structure with an X-brace in the side position is upper than that of a structure with 6-story with an X-brace in the corner and the natural frequency of a structure with an X-brace in the side position is lower than that of a structure with 9 and 12-story with an X-brace in the corner.

Eccentricity (mm)	Building ID	Frequency cyc/sec	Building ID	Frequency cyc/sec	Building ID	Frequency cyc/sec	Building ID	Frequency cyc/sec	Building ID	Frequency cyc/sec	Building ID	Frequency cyc/sec
	SC6-B12-1	0.821	SC9-B12-1	0.506	SC12-B12-1	0.349	SS6-B12-1	0.864	SS9-B12-1	0.500	SS12-B12-1	0.346
	SC6-B15-1	0.862	SC9-B15-1	0.526	SC12-B15-1	0.359	SS6-B15-1	0.894	SS9-B15-1	0.516	SS12-B15-1	0.354
0	SC6-B16-1	0.873	SC9-B16-1	0.531	SC12-B16-1	0.362	SS6-B16-1	0.901	SS9-B16-1	0.521	SS12-B16-1	0.356
	SC6-B20-1	0.903	SC9-B20-1	0.548	SC12-B20-1	0.371	SS6-B20-1	0.925	SS9-B20-1	0.534	SS12-B20-1	0.363
	SC6-B25-1	0.931	SC9-B25-1	0.564	SC12-B25-1	0.379	SS6-B25-1	0.946	SS9-B25-1	0.546	SS12-B25-1	0.369
	SC6-B12-2	0.789	SC9-B12-2	0.490	SC12-B12-2	0.340	SS6-B12-2	0.793	SS9-B12-2	0.484	SS12-B12-2	0.337
	SC6-B15-2	0.820	SC9-B15-2	0.504	SC12-B15-2	0.348	SS6-B15-2	0.819	SS9-B15-2	0.496	SS12-B15-2	0.343
500	SC6-B16-2	0.829	SC9-B16-2	0.509	SC12-B16-2	0.350	SS6-B16-2	0.826	SS9-B16-2	0.500	SS12-B16-2	0.345
	SC6-B20-2	0.857	SC9-B20-2	0.521	SC12-B20-2	0.357	SS6-B20-2	0.846	SS9-B20-2	0.509	SS12-B20-2	0.350
	SC6-B25-2	0.884	SC9-B25-2	0.534	SC12-B25-2	0.363	SS6-B25-2	0.863	SS9-B25-2	0.518	SS12-B25-2	0.354
	SC6-B12-3	0.639	SC9-B12-3	0.409	SC12-B12-3	0.292	SS6-B12-3	0.648	SS9-B12-3	0.409	SS12-B12-3	0.292
	SC6-B15-3	0.661	SC9-B15-3	0.421	SC12-B15-3	0.299	SS6-B15-3	0.669	SS9-B15-3	0.419	SS12-B15-3	0.298
1000	SC6-B16-3	0.668	SC9-B16-3	0.424	SC12-B16-3	0.301	SS6-B16-3	0.676	SS9-B16-3	0.422	SS12-B16-3	0.300
	SC6-B20-3	0.690	SC9-B20-3	0.435	SC12-B20-3	0.307	SS6-B20-3	0.694	SS9-B20-3	0.431	SS12-B20-3	0.305
	SC6-B25-3	0.711	SC9-B25-3	0.446	SC12-B25-3	0.313	SS6-B25-3	0.711	SS9-B25-3	0.439	SS12-B25-3	0.309
	SC6-B12-4	0.518	SC9-B12-4	0.336	SC12-B12-4	0.244	SS6-B12-4	0.529	SS9-B12-4	0.338	SS12-B12-4	0.245
	SC6-B15-4	0.536	SC9-B15-4	0.345	SC12-B15-4	0.250	SS6-B15-4	0.545	SS9-B15-4	0.346	SS12-B15-4	0.250
1500	SC6-B16-4	0.542	SC9-B16-4	0.349	SC12-B16-4	0.252	SS6-B16-4	0.551	SS9-B16-4	0.349	SS12-B16-4	0.252
	SC6-B20-4	0.571	SC9-B20-4	0.357	SC12-B20-4	0.257	SS6-B20-4	0.566	SS9-B20-4	0.357	SS12-B20-4	0.257
	SC6-B25-4	0.576	SC9-B25-4	0.366	SC12-B25-4	0.262	SS6-B25-4	0.581	SS9-B25-4	0.364	SS12-B25-4	0.261

Table 10: Natural frequency of all buildings.

Eccentricity (mm)	Building ID	Period sec	Building ID	Period sec	Building ID	Period sec	Building ID	Period sec	Building ID	Period sec	Building ID	Period sec
	SC6-B12-1	1.218	SC9-B12-1	1.974	SC12-B12-1	2.863	SS6-B12-1	1.157	SS9-B12-1	1.997	SS12-B12-1	2.890
	SC6-B15-1	1.160	SC9-B15-1	1.900	SC12-B15-1	2.780	SS6-B15-1	1.118	SS9-B15-1	1.935	SS12-B15-1	2.820
0	SC6-B16-1	1.145	SC9-B16-1	1.880	SC12-B16-1	2.758	SS6-B16-1	1.109	SS9-B16-1	1.918	SS12-B16-1	2.802
	SC6-B20-1	1.107	SC9-B20-1	1.822	SC12-B20-1	2.694	SS6-B20-1	1.081	SS9-B20-1	1.871	SS12-B20-1	2.750
	SC6-B25-1	1.073	SC9-B25-1	1.771	SC12-B25-1	2.637	SS6-B25-1	1.057	SS9-B25-1	1.831	SS12-B25-1	2.706
	SC6-B12-2	1.266	SC9-B12-2	2.039	SC12-B12-2	2.935	SS6-B12-2	1.261	SS9-B12-2	2.062	SS12-B12-2	2.965
	SC6-B15-2	1.219	SC9-B15-2	1.981	SC12-B15-2	2.869	SS6-B15-2	1.221	SS9-B15-2	2.014	SS12-B15-2	2.910
500	SC6-B16-2	1.205	SC9-B16-2	1.964	SC12-B16-2	2.850	SS6-B16-2	1.210	SS9-B16-2	2.000	SS12-B16-2	2.895
	SC6-B20-2	1.166	SC9-B20-2	1.916	SC12-B20-2	2.797	SS6-B20-2	1.182	SS9-B20-2	1.963	SS12-B20-2	2.854
	SC6-B25-2	1.131	SC9-B25-2	1.872	SC12-B25-2	2.748	SS6-B25-2	1.158	SS9-B25-2	1.930	SS12-B25-2	2.818
	SC6-B12-3	1.564	SC9-B12-3	2.443	SC12-B12-3	3.417	SS6-B12-3	1.541	SS9-B12-3	2.443	SS12-B12-3	3.421
	SC6-B15-3	1.511	SC9-B15-3	2.375	SC12-B15-3	3.339	SS6-B15-3	1.494	SS9-B15-3	2.384	SS12-B15-3	3.353
1000	SC6-B16-3	1.495	SC9-B16-3	2.354	SC12-B16-3	3.314	SS6-B16-3	1.479	SS9-B16-3	2.366	SS12-B16-3	3.332
	SC6-B20-3	1.449	SC9-B20-3	2.296	SC12-B20-3	3.249	SS6-B20-3	1.440	SS9-B20-3	2.318	SS12-B20-3	3.277
	SC6-B25-3	1.405	SC9-B25-3	2.242	SC12-B25-3	3.187	SS6-B25-3	1.405	SS9-B25-3	2.274	SS12-B25-3	3.228
	SC6-B12-4	1.927	SC9-B12-4	2.971	SC12-B12-4	4.090	SS6-B12-4	1.889	SS9-B12-4	2.955	SS12-B12-4	4.071
	SC6-B15-4	1.864	SC9-B15-4	2.891	SC12-B15-4	3.997	SS6-B15-4	1.832	SS9-B15-4	2.882	SS12-B15-4	3.986
1500	SC6-B16-4	1.844	SC9-B16-4	2.865	SC12-B16-4	3.966	SS6-B16-4	1.814	SS9-B16-4	2.859	SS12-B16-4	3.959
	SC6-B20-4	1.749	SC9-B20-4	2.795	SC12-B20-4	3.886	SS6-B20-4	1.766	SS9-B20-4	2.797	SS12-B20-4	3.888
	SC6-B25-4	1.735	SC9-B25-4	2.728	SC12-B25-4	3.808	SS6-B25-4	1.721	SS9-B25-4	2.740	SS12-B25-4	3.828

Table 11: Period of all buildings.

Regarding structural performance, modifying the bracing section increases ultimate loads while slightly decreasing displacement. Changing the bracing section area in an eccentric frame influences the stresses at failure, the displacement at failure, and the ductility value. Greater bracing area results in higher ultimate pressures but lower ultimate displacement and less ductility. Almost all buildings need to be designed to disperse energy when earthquakes occur. They need to disperse the energy without compromising the structure's integrity so that the stresses from earthquakes and gravity may be transferred to the foundation. Modern performance-based seismic engineering in steel structures has several design goals. Eccentric X-braces are a beneficial structural component of an appropriate structural typology for accomplishing these goals. In order to resist severe earthquakes, buildings need a frame structure with high lateral strength and stiffness and good energy dissipation capabilities. Regarding strength and flexibility, eccentric X-braces are hard to beat. They feature the best of both moment-resisting and concentrically braced frames. The first computational studies of typical eccentrically braced structures subjected to lateral static stresses found that eccentric X-braces were better at handling earthquakes.

CONCLUSIONS

Our findings on how eccentricity and cross-section of X-braces influence the performance of steel frame multi-story structures were analyzed using the latest version of the ETABS program. Possible conclusion:

- In multi-story buildings with six stories, the eccentric X-brace is more effective in preventing top-story displacement than in buildings with 9 or 12 stories.
- The stability and ductility of the eccentrically braced frame were affected by the length of the horizontal links (eccentricity), which reflected the system's energy dissipation capability.
- The efficiency of shear-yielding is influenced by the shear in the links, which is affected by the shear in the story. Shorter horizontal link lengths with small eccentricities are more effective in achieving shear-yielding efficiency. However, longer links with large eccentricities may experience bending.
- The lateral rigidity of eccentric X-brace frames is lower than that of concentrically braced frames, particularly when diagonal bracing is used. However, the eccentricity-induced stiffness loss may be recovered by increasing the cross-section area of the X-braced component.
- The ductility of an eccentric brace frame (EBF) changes noticeably as the X-brace section and eccentricity change because EBFs absorb more energy and move more horizontally.
- The ultimate load, ultimate displacement, and ductility values of all eccentric frame types are sensitive to the bracing section's area. While increasing the ultimate loads, increasing the ultimate bracing section size reduces the ultimate displacement and ductility values. Under seismic stresses, most buildings should be built to disperse energy.
- This investigation showed that the finite element model could provide reliable predictions of EBF behavior. ETABS analysis and experimental findings were in excellent accord. The ETABS model successfully captured all of the critical features of the chosen structures.

REFERENCES

[1] Naidoo, P. and Drosopoulos, G. (2020). Evaluation of the dynamic response of structures using auxetic-type base isolation, Frattura ed Integrità Strutturale, 51, pp. 52-70. DOI: 10.3221/IGF-ESIS .51.05.

[2] Souri, O. and Mofid, M. (2023). Seismic evaluation of concentrically braced steel frames equipped with yielding elements and BRBs, Results in Engineering, 17, 100853. DOI:10.1016/j.rineng. 2022.100853.

[3] Annan, C., Youssef, M. and El Naggar, M. (2009). Experimental evaluation of the seismic performance of modular steel-braced frames, Engineering Structures, 31, pp. 1435-1446. DOI: 10.1016/j.engstruct.2009.02.024.

[4] Unal, A. and Kaltakci, M. (2016). Seismic behavior of concentrically steel braced frames and their use in strengthening of reinforced concrete frames by external application, Steel and Composite Structures, 21(4), pp. 687-702. DOI:10.12989/scs.2016.21.4.687.

[5] Popov, E., Kasai, K. and Engelhardt, M. (1986). Advances in design of eccentrically braced frames, Bulletin of the New Zealand Society for Earthquake Engineering, 20(1), pp. 22-29. DOI: 10.5459 /bnzsee.20.1.22-29.

[6] Bekdaş, G. and Nigdeli, S. (2017). Metaheuristic based optimization of tuned mass dampers under earthquake excitation by considering soil-structure interaction, Soil Dynamics and Earthquake Engineering, 92, pp. 443-461. DOI: 10.1016/j.soildyn.2016.10.019.

[7] Brandão, F., Diógenes, A., Fernandes, J., Mesquita, E. and Betti, M. (2018). Seismic behavior assessment of a Brazilian heritage construction, Frattura ed Integrità Strutturale, 12(45), p. 14-32. DOI: 10.3221/IGF-ESIS.45.02.

[8] Stratan, A., Dogariu, A. and Dubina, D. (2007). Bolted links for eccentrically braced frames: Influence of link stiffness, Proceedings of the 3rd International Conference on Steel and Composite Structures, ICSCS07 - Steel and Composite Structures, pp. 847-853.

[9] Harba, I., Abdulridha, A. and ALShaar, A. (2023). Numerical analysis of reinforced concrete circular columns strengthening with CFRP under concentric and eccentric loadings, Frattura ed Integrità Strutturale, 63, pp. 190-205. DOI: 10.3221/IGF-ESIS.63.16.

[10] Boursas, F. and Boutagouga, D. (2021). Parametric study of I-shaped shear connectors with different orientations in pushout test, Frattura ed Integrità Strutturale, 15(57), pp. 24-39. DOI: 10.3221/IGF-ESIS.57.03.

[11] Bouaricha, A., Handel, N., Boutouta, A. and Djouimaa, S. (2021). Load bearing capacity of thin-walled rectangular and Ishaped steel sections of short both empty and concrete-filled columns, Frattura ed Integrità Strutturale, 15(58), pp. 77-85. DOI: 10.3221/igf-esis.58.06.

[12] Sadeghi, A., Kazemi, H. and Samadi, M. (2021). Reliability and Reliability-based Sensitivity Analyses of Steel Moment-Resisting Frame Structure subjected to Extreme Actions, Frattura ed Integrità Strutturale, 57, pp. 138-159. DOI: 10.3221/IGF-ESIS.57.12.

[13] Razavi, S., Peron, M., Torgersen, J., Berto, F. and Mutignani, F. (2017). Effect of hot dip galvanization on the fatigue strength of steel bolted connections, Frattura ed Integrità Strutturale, 41, pp. 432-439. DOI: 10.3221/IGF-ESIS.41.54.

[14] Yi, T-H., Li, H-N., Song, G. and Zhang, X-D. (2015). Optimal sensor placement for health monitoring of high-rise structure using adaptive monkey algorithm, Structural Control and Health Monitoring, 22(4), pp. 667-681. DOI:10.1002/stc.1708.

[15] Sun, H., Mordret, A., Prieto, G., Toksöz, M. and Büyüköztürk, O. (2017). Bayesian characterization of buildings using seismic interferometry on ambient vibrations, Mechanical Systems and Signal Processing, 85, pp. 468-486. DOI: 10.1016/j.ymssp.2016.08.038.

[16] Harba, I. and Abdulridha, A. (2017). Finite Element Analysis of RC Tapered Beams under Cyclic Loading, Al-Nahrain Journal for Engineering Sciences, 20(2), pp. 378–396. https://nahje.com/index.php/main/article/view/117.

[17] Abdulridha, A., Risan, H. and Harba, I. (2018). Numerical Analysis of Two-Way RC Slab with a Sawn Up Opening Strengthened by CFRP, International Journal of Civil Engineering and Technology, 9(8), pp. 1159-1167.

[18] Skolnik, D., Lei, Y., Yu, E. and Wallace, J-W. (2006). Identification, model updating, and response prediction of an instrumented 15-story steel-frame building, Earthquake Spectra, 22(3). DOI: 10.1193 /1.2219487.

[19] Abdulridha, A., Taki, Z. and Harba, I. (2018). Numerical Analysis of Reinforced Concrete Beam Strengthened by Cfrp Subjected to Monotonic Loading, International Journal of Civil Engineering and Technology, 9(10), pp. 894–904. https://iaeme.com/Home/article_id/IJCIET_09_10_091.

[20] Harba, I., Abdulridha, A. and AL-Shaar, A. (2022). Numerical analysis of high-strength reinforcing steel with conventional strength in reinforced concrete beams under monotonic loading, Open Engineering, 12(1), pp. 817-833. DOI: 10.1515/eng-2022-0365.

[21] Zhu, B. and Frangopol, D. (2013). Reliability assessment of ship structures using Bayesian updating, Engineering Structures, 56(7), pp. 1836-1847. DOI: 10.1016/j.engstruct.2013.07.024.

[22] European committee for standardization. (2004). EUROCODE 8: Design of structures for earthquake resistance – Part 1: General rules, seismic actions and rules for buildings, British Standards Institution.
[23] American Institute of Steel Construction. (2016). Seismic Provisions for Structural Steel Buildings, American Institute of Steel Construction.
[24] Goggins, J. and Salawdeh, S. (2013). Validation of nonlinear time history analysis models for single-storey concentrically braced frames using full-scale shake table tests, Earthquake Engineering and Structural Dynamics 42(8), pp. 1151-1170. DOI:10.1002/eqe.2264.
[25] Uang, C. and Bruneau, M. (2018). State-of-the-Art Review on Seismic Design of Steel Structures, Journal of Structural Engineering, 144(4), 03118002. DOI: 10.1061/ (ASCE) ST.1943-541X.0001973.
[26] Canadian Standards Association. (2019). Standards Council of Canada. Design of Steel Structures, CSA Group: Toronto, Canada.
[27] Marino, E., Nakashima M. and Mosalam, K. (2005). Comparison of European and Japanese seismic design of steel building structures, Engineering Structures, 27(6), pp. 827-840. DOI: 10.1016/j. engstruct.2005.01.004.
[28] Shi, Q., Yan, S., Wang, X., Sun, H. and Zhao, Y. (2020). Seismic Behavior of the Removable Links in Eccentrically Braced Frames with Semirigid Connections, Advances in Civil Engineering, (2), pp. 1-26. DOI: 10.1155/2020/9405107.
[29] Bozkurt, M., Azad, S. and Topkaya, C. (2018). Low-Cycle Fatigue Testing of Shear Links and Calibration of a Damage Law, Journal of Structural Engineering 144(10), 04018189. DOI: 10.1061/ (ASCE) ST.1943-541X.0002192.
[30] Popov, E. and Engelhardt, M. (1988). Seismic eccentrically braced frames, Journal of Constructional Steel Research, 10, pp. 321-354.
[31] Popov, E., Engelhardt, M. and Ricles, J. (1989). Eccentrically braced frames: United-States practice, Engineering Journal, American Institute of Steel Construction, 26, pp. 66-80.
[32] Sullivan, T. (2013). Direct displacement-based seismic design of steel eccentrically braced frame structures, Bulletin of Earthquake Engineering, 11(6), pp. 2197-2231. DOI: 10.1007/s10518-013-9486-8.
[33] Ghobarah, A. and Abou Elfath, H. (2001). Rehabilitation of a reinforced concrete frame using eccentric steel bracing, Engineering Structures, 23, pp. 745-755. DOI: 10.1016/S0141-0296(00)00100-0.
[34] Jain, A., Goel, S. and Hanson, R. (1980). Hysteretic cycles of axially loaded steel members, Journal of the Structural Division, 106(8), pp. 1777-1795. DOI: 10.1061/JSDEAG.0005498.
[35] Kahn, L. and Hanson, R. (1976). Inelastic cycles of axially loaded steel members, Journal of the Structural Division, 102(5), pp. 947-959. DOI: 10.1061/JSDEAG.0004355.
[36] Lee, P. and Noh, H. (2010). Inelastic buckling behavior of steel members under reversed cyclic loading, Engineering Structures, 32(9), pp. 2579-2595. DOI: 10.1016/j.engstruct.2010.04.031.
[37] Popov, E. and Black, R. (1981). Steel struts under severe cyclic loadings, Journal of the Structural Division, 107(9), pp. 1857-1881. DOI: 10.1061/JSDEAG.0005786.
[38] Salawdeh, S. and Goggins, J. (2013). Numerical simulation for steel brace members incorporating a fatigue model, Engineering Structures, 46, pp. 332-349. DOI: 10.1016/j.engstruct.2012.07.036.
[39] Tremblay, R., Archambault, M. and Filiatrault, A. (2003). Seismic response of concentrically braced steel frames made with rectangular hollow bracing members, Journal of Structural Engineering, 129(12), pp. 1626-1636. DOI: 10.1061/ (ASCE) 0733-9445(2003)129:12(1626).
[40] Tremblay, R., Lacerte, M. and Christopoulos, C. (2008). Seismic response of multistory buildings with selfcentering energy dissipative steel braces, Journal of Structural Engineering, 134(1), pp. 108-120. DOI: 10.1061/(ASCE)0733-9445(2008)134:1(108).
[41] Fell, B., Kavinde, A., Deierlein, G. and Myers, A. (2009). Experimental Investigation of Inelastic Cyclic Buckling and Fracture of Steel Braces, Journal of Structural Engineering, 135(1), pp. 19-32. DOI: 10.1061/(ASCE)0733-9445(2009)135:1(19).
[42] Nip, K., Gardner, L. and Elghazouli, A. (2010). Cyclic testing and numerical modelling of carbon steel and stainless steel tubular bracing members, Engineering Structures, 32(2), pp. 424-441. DOI: 10.1016/j.engstruct.2009.10.005.
[43] Haddad, M., Brown, T. and Shrive, N. (2011). Experimental cyclic loading of concentric HSS Braces, Canadian Journal of Civil Engineering, 38(1), pp. 110-123. DOI: 10.1139/L10-113.
[44] Ureña, A., Tremblay, R. and Rogers, C. (2022). Experimental and numerical study of square HSS BIEs under cyclic loading, Engineering Structures, 252, 113669. DOI:10.1016/j.engstruct.2021.113669.
[45] Lotfollahi, M., Alinia, M. and Taciroglu, E. (2016). Validated finite element techniques for quasi-static cyclic response analyses of braced frames at sub-member scales, Engineering Structures, 106, pp. 222-242. DOI: 10.1016/j.engstruct.2015.07.049.

[46] Center for Engineering Strong Motion Date. (n.d). CESMD Strong-Motion Data Set. Available at: https://strongmotioncenter.org/cgi-bin/CESMD/archive.pl.
[47] CSI. (2020). ETABS Software Version 2020, Computers ans structures, inc.
[48] ASCE 7-22. (2022). Minimum Design Loads and Associated Criteria for Buildings and Other Structures: ASCE/SEI 7-22, American Society of Civil Engineers, Reston, Virginia.
[49] Unal, A. and Kaltakci, M. (2016). Seismic behavior of concentrically steel braced frames and their use in strengthening of reinforced concrete frames by external application, Steel and Composite Structures, 21(4), pp. 687-702. DOI: 10.12989/scs.2016.21.4.687.
[50] Harba, I. and Abdulridha, A. (2021). Numerical analysis of RC columns under cyclic uniaxial and biaxial lateral load, Građevinar, 73 (10), pp. 979-994, DOI: 10.14256/JCE.2889.2020
[51] Risan, H., Harba, I. and Abdulridha, A. (2017). Numerical analysis of RC wall with opening strengthened by CFRP subjected to eccentric loads, Građevinar, 69 (7), pp. 573-580, DOI: 10.14256/JCE.1707.2016
[52] Abolfazl, A. and Imanpour, A. (2021). Seismic response of steel multi-tiered eccentrically braced frames, Journal of Constructional Steel Research, 181, 106600. DOI:10.1016/j.jcsr.2021.106600.
[53] Tian, X., Su, M., Lian, M., Wang, F. and Li, F. (2018). Seismic behavior of K-shaped eccentrically braced frames with high-strength steel: Shaking table testing and FEM analysis, Journal of Constructional Steel Research, 143, pp. 250-263. DOI:10.1016/j.jcsr.2017.12.030.
[54] Wang, F., Su, M., Hong, M., Guo, Y. and L, S. (2016). Cyclic behaviour of Y-shaped eccentrically braced frames fabricated with high-strength steel composite, Journal of Constructional Steel Research, 120, pp. 176-187. DOI://10.1016/j.jcsr.2016.01.007.